석 . 박사 학위논문 등표지

	Electrospray Deposition of Functional Thin Films – Fabrication and Characterization• **Nauman M. Muhammad • 2012**	

ATHESIS

FOR THE DEGREE OF DOCTOR OF PHILOSOPHY

Electrospray Deposition of Functional Thin Films – Fabrication and Characterization

Nauman Malik Muhammad

Department of Mechatronics Engineering

GRADUATESCHOOL

JEJUNATIONALUNIVERSITY

2012. 08

Electrospray Deposition of Functional Thin Films – Fabrication and Characterization

Nauman Malik Muhammad

(Supervised by Professor Kyung Hyun Choi)

A thesis submitted in partial fulfillment of the requirement for the degree of Doctor of Philosophy

2012. 08

The thesis has been examined and approved.

.....

Thesis Director, Chul-Ung Kang, Professor, Department of Mechatronics Engineering

.....

Yang-Hoi Doh, Professor, Department of Electronic Engineering

.....

Jin-Ho Bae, Professor, Department of Ocean System Engineering

.....

Kyung-Hyun Choi, Professor, Department of Mechatronics Engineering

.....

Piljoong Kang, Ph.D., Samsung Electro-Mechanics Company Limited

.....

Date

Department of Mechatronics Engineering
GRADUATESCHOOL
JEJUNATIONALUNIVERSITY
REPUBLIC OF KOREA

To

PAKISTAN-My First love

Acknowledgements

Start with the name of Almighty Allah, the most merciful, the most beneficent. First of all I would present my humble gratitude in front of Allah Who enabled me to accomplish the dignified cause of education and learning and I would pray to Him that He would make me able to utilize my knowledge and edification for the betterment of humanity and its development. At this important occasion when I am going to get the highest educational degree, I acknowledge and salute the vision and support of my father who prophesized this moment many years back. The prayers of my mother and her confidence in me were a source of constant support during the course of my degree.

I feel extremely lucky to have Prof. Kyung Hyun Choi as my PhD supervisor and will always be indebted of him for all his kind support, supervision, and favors and in making me what I am today. The way he identified the best in me and made me use it during these three years speaks of itself of his man management skills, his persona and his thorough professionalism. His thought-provoking seminars and discussions and a never-ending appetite for excellence I will admire and cherish forever. His encouragement and guidance during my high time and support and kindness during the down times have all been a source of motivation towards learning more and more. I am also thankful to Prof. Chul-Ung Kang for being my thesis advisor and Prof. Yang HuiDoh, Professor Jin Ho Bae and Dr. Phil-Jeong Kang for being my thesis advisors. Their help and support in my thesis completion is highly gratified. I would also like to thank Prof. Kyung Ho Cho, Prof. Sang Jae Kim, Prof. Dong Won Jung and Prof. Hyun MyungTaek for their extremely useful and pensive lectures.

During my stay I had many mentors who helped a lot in making myself more organized, disciplined and efficient. Dr. UmerZeeshanIjaz, Dr. Ahmar Rashid, Dr. Khalid Rahman, Dr. Anil Kumar, Dr. Rajneesh Mohan, Dr. SrikantSaini,Asif Ali Rehmani and Rongli Wang are a few of those whose friendship, help and support I would always admire. Friends are a blessing and I couldn't imagine spending long years in Jeju without friendly company. I am especially thankful to Navaneethan for

his sustenance and respect he has given to me. Arshad, Kamran, Naeem, Ahsan, Hyun-Woo, Maria, Ganesh, Farrukh, Zubair, Murtuza, Adnan, Jeong-beom, Hyung Chan, Go-beom, Karthik, Anand, Sarwan, Safdar and Shoaib are a few names whose support were always there for me. I am thankful to Kyung-Hyun Lee, Jae-he Park and Ji-yeon for their always helping presence around me.

At the end I would thank my lovely wife and beloved son for coping with me during these tough years. The successful completion of my PhD is in fact the result of their presence and overwhelming support whenever I needed it the most.

Contents

List of Figures

List of Tables

ABSTRACT

Electrospray deposition (ESD) process is capable of spraying and depositing various substances such as organic/inorganic compounds and/or synthetic polymers. ESD process can maintain the sample relatively free from damage, since the whole procedure is conducted under room temperature and atmospheric pressure. Fabrication of nano-sized particles and fibers and deposition in a large area are possible. This is the first account where ESD is being utilized for different functional materials' deposition, and the films are characterized thoroughly taking ESD in competition to the existing thin film deposition techniques like chemical vapour deposition, plasma related techniques and physical vapour deposition techniques. Although many scientists and researchers have adopted ESD as their research topic, ESD has been only utilized in mass spectroscopy and powder production applications. In this thesis three different types of thin films are deposited via ESD and characterized thoroughly making them perfectly suitable for their use in device fabrication. First Copper Indium diSelenide (CIS) ,which is a direct bandgap semiconductor useful for manufacturing solar cells is deposited. CIS nano-particles, manufactured through solvo-thermal process are dissolved in Ethanol:Terpineol solution, and six different types of inks are prepared on the basis of different solvent composition and particle concentration. Fabricated layers are characterized for their purity, morphology, optical, structural and electrical properties, and an optimum ink is identified.

In the second phase of the thesis, Zinc Oxide (ZnO), which is a wide-bandgap n-type semiconductor of the II-VI semiconductor group, thin films are fabricated via ESD. ZnO nano particle ink is first prepared by dissolving the nanoparticles in Ethanol, and Triton is used as a surfactant. The ink is then subjected to ESD to fabricate ~120 nm thick films

which are characterized for their surface morphology, phase, purity and optical & electrical properties thereby elucidating ESD as a cheap and easy alternative to the conventional thin film deposition processes.

In the last part of this study, transparent conductive oxide films i.e. Aluminum doped Zinc Oxide (ZnO:Al) films are fabricated and characterized in the same way as ZnO films. The fabricated films in this thesis compete with the ones made by different intricate and expensive conventional systems. The main advantage is that ESD process precludes the use of high vacuum systems therefore making the process cheap and simple. Also material wastage is very small, and inks used in the process are completely inert to the environment thereby making the process and clean and green.

1. Introduction

1.1 Functional Thin Films

Functional thin films are the coatings, deposited directly on substrates for purposes other than merely appearance. Functional thin films are fabricated for variety of purposes ranging from conductive to non-conductive surface manifestation, passivation, anti-reflective coatings and window layers etc. Practically speaking, athin film is a layer of material ranging from fractions of a nanometer (monolayer) to several micrometers in thickness. Electronic semiconductor devices and optical coatings are the main applications benefiting from thin films.A very common application of thin films is the household mirror, which typically has a thin metal coating on the back of a sheet of glass to form a reflective interface. The process of silvering was once commonly used to produce mirrors. A periodic structure of alternating thin films of different materials may collectively form a so-called superlattice which exploits the phenomenon of quantum confinement by restricting electronic phenomena to two-dimensions. Apart from these, work is being done with ferromagnetic and ferroelectric [Liakhova et al. 2006] thin films for use as computer memory. Thin films are also being applied to pharmaceuticals, where they are used in the thin film drug delivery systems. Thin-films are also used to produce thin-film batteries, solar cells and organic light emitting diodes.

Ceramic thin films are also in wide use these days. The relatively high hardness and inertness of ceramic materials make this type of thin coating of interest for protection of substrate materials against corrosion, oxidation and wear. In particular, the use of such coatings on cutting tools can extend the life of these items by several orders of magnitude. Thermal barrier coatings are also an application area where thin films are working wonders in modern aviation equipments. A new class of thin film inorganic oxide materials, called amorphous heavy-metal cation multi-component oxides have been recently introduced, which could be used to make transparent transistors that are inexpensive, stable, and environment friendly[Chiang & Wagner 2005]. Metal oxide thin films e.g. intrinsic and doped Zinc Oxide, Indium Tin Oxide, Titanium oxide, Zirconium Oxide and Silicon Oxide etc are very attractive research topics

because of their excellent electrical properties and stability and are extensively being used in thin film devices like transistors, radio frequency identification tags, light emitting diodes, memory devices like memristors and programmable metallization cells and solar cells etc. Thin film solar cells are also main beneficiary of thin films as second, third and 4^{th} generation solar cells are built as a layer by layer structure. Both inorganic e.g Copper Indium diSelenide and Cadmium Telluride type and organic, having Poly(3-hexylthiophene-diyl) active layers are deposited using thin film techniques where thin film thickness is in microns.

1.2 Conventional Deposition Techniques

Thin films, with all their importance and applications are a very attractive topic in the field of process engineering and material physics. Hence many a methods are available conventionally, with their peculiar advantages and disadvantages, for the fabrication of thin films. We will hereby discus most important of them with their benefits and limitations, thereby making a case for suggesting a new method for the successful fabrication of thin films, known as electrospray deposition which is the topic of present study.

Atomic Layer Deposition

One of the most attractive techniques for pure and high quality thin films is that of atomic layer deposition (ALD). It is usually used to produce thin layer coatings having excellent barrier properties. ALD is being employed commercially by Solar cell and display. ALD is a surface controlled layer-by-layer thin film deposition process based on self-terminating gas-solid reactions usually applied to create thin nano-layers of metal oxides. With the advent of modern technology, it has become possible to develop high barrier polymer films using ALD mainly synthetic and bioplastic films and coatings achieving good barrier properties against moisture and oxygen [Hirvikorpi et al. 2010]. The main drawback associated with ALD is the requirement of very high vacuum during the process, very very clean environment and very costly and intricate equipment. Also the limitations like large area deposition and continuous deposition are also there.

Chemical Vapor Deposition

Although CVD normally utilizes high temperatures not suitable for heat sensitivematerials, modified CVD can be also used to produce thin polymeric films on different substrates. Initiated chemical vapor deposition (iCVD) can be used to produce linear polymers. iCVD has been used to polymerize vinyl monomers. Gases are fed into a vacuum chamber where heated wires are used to decompose the initiatorinto free radicals [Bakker et al. 2007]. The polymerization on the surface of a cooled substrate will then proceed as free radical polymerization. Oxidative CVD on the other hand relies on step growth polymerization employing an oxidant and is used for the deposition of thin films of conducting polymers [Bakker et al. 2007].

Plasma Deposition Techniques

While plasma depositions are usually made at low pressure, recent research is directed towards coating at atmospheric pressure, simply because it can be implemented as part of an in-line processes. In atmospheric plasma, ionized gas and radicals are separately produced from a mixture of the carrier gas and chemical precursor and blown onto a substrate. A typical application is the deposition of siloxanes for their barrier, hydrophobic and release properties. The main challenges are related to the complex reactions in the plasma and the deposition speed and uniformity. Main disadvantages here as well are high temperatures involved, vacuum systems and costly equipment in addition, presence of clean environment system isolation involving intricacies are also great challenges.

Liquid Flame Spraying

Liquid flame spraying, an aerosol method, has been suggested as a tool for creating and applying nano-particles and nano-coatings on various flexible substrates, such as paper, paperboard and polymer films [Tenhaeff& Gleason 2008, Makela et al. 2009]. The idea is to feed small droplets of liquid precursors through a spray nozzle into a flame. While the flame temperature is high, the thermal load on the surface is 100

–300 °C. Different gases can be used to create the flame. The droplets evaporate and the precursors may react to form nanoparticles. The gas and particle flow is then subjected to the surface to be coated. Functional properties provided could be conductivity or barrier properties. Increased line speed decreases the thermal effect on the substrate. For example, nano TiO_2 is used for hydrophobicity and SiO_2 for hydrophilicity. Main challenges involved in this simple mehod are high temperatures, high temperature sustaining materials' requirements and limitation of usable substrates.

Miscellaneous techniques

In addition to the methods listed above, there is a whole set of engineered biohybridcoatings. In these coatings enhanced properties are achieved by combining chemoenzymaticmodification methods with organized coating structures or formation of controlled assemblythrough high shear deposition. This allows interesting combinations of biopolymers andnanoparticles for e.g. barrier purposes.

There are thus several alternatives for creating nano coatings or coatings utilizing nanoscalefeatures. Techniques, such as ALD, provide possibilities to enhance the properties ofvarious sensitive materials including papers, polymer films and coated papers and boards.

1.3 Electrospray Deposition and its Applications

As the name suggests, the deposition phenomenon should solely be a spray achieved through electrostatic forces. In fact it is an imbalance between the surface forces arising because of the surface tension of the liquid to be sprayed and Maxwell stresses which are induced because of the electric field, that pull the liquid downwards from the capillary into a stable jet which further disintegrates into smaller droplets because of coulomb forces and hence a cloud of charged, mono-dispersed and extremely diminutive (sometimes up to nanometers) droplets is achieved. A typical electrospray deposition phenomenon consists of following sequence [J. Makela 2010]:

1. Spray formation at the Taylor-cone tip
2. Droplet transport from nozzle to substrate with evaporation of solvent and disruption of droplets at the mid of spray stream
3. Preferential landing on the substrate/ground, and
4. Droplet spreading, penetration and partial drying

An important aspect of electrospray is that droplet agglomeration does not exist at all as the charged droplets are self-dispersing in the space due to mutual Coulomb repulsion. The charge and size of the droplets can be controlled to some extent by adjusting the liquid flow rate and the voltage applied to the nozzle.

Before the spray actually happens, a stable Taylor cone[Chen &Schoonman 2004] is to be achieved which ultimately ejects the spray. A stable, uniform and symmetric Taylor cone at the onset of capillary exit is the guarantee of a smooth and stable electrospray. Important parameters related to Taylor cone formation are the critical onset voltage and liquid flow rate along with liquid physical properties and stand-off distance. A complete description on this aspect of electrohydrodynamics can be found in the next chapter.

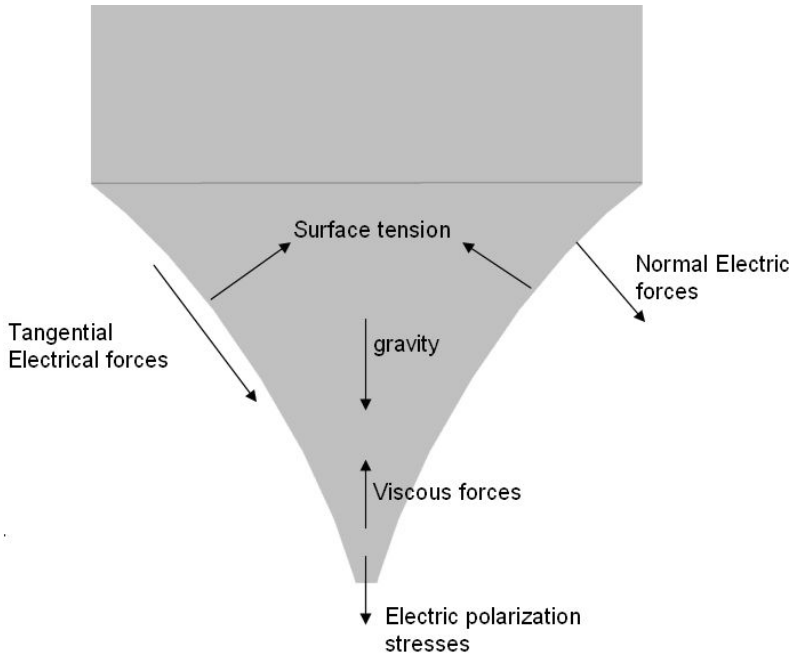

Figure 1-1. Body-force diagram of the Taylor-cone.

If a body force diagram for the fluid in a capillary problem, as shown in Figure 1, is looked closely at, three main contributing forces will be witnessed. First is the surface tension force, P_s which will oppose the generation of meniscus and hence the jet formation, secondly the hydrostatic pressure, P_h, which will pull the meniscus downwards and lately, the electrostatic pressure P_e, is the deciding force which acts tangentially at the meniscus and the amalgam of these forces finally gets the required jet. When put in the equation form, we get

$$P_h + P_s + P_e = 0 \tag{1-1}$$

where

$$P_h = \rho_l g \Delta H \tag{1-2}$$

$$P_e = E_{ds}^2 / 2\varepsilon_r \tag{1-3}$$

ΔH is the liquid level difference between the container and the free end of the nozzle and ε_r is the relative permittivity of the liquid to vacuum permittivity [Chen &Schoonman 2004]. The flow rate is required to compensate fluid in the meniscus, which is directly proportional to the backflow of fluid due to the electrical stress. Thus, the governing force for the ejection of the droplet is electrostatic force since the flow rate is provided to maintain the steady level of ink at the orifice outlet, whereas the gravitational force has little contribution due to the high fluidic resistance in the micro-channel as the capillary diameter is very small and the surface tension of the liquid will add to the fluidic resistance.

ESD finds it applications almost everywhere where the competing technologies are applicable. From printed electronics to powder production, from nuclear instruments to solar cells, from Li batteries to fuel cells and bio-applications, ESD has been in the limelight since its inception. A very comprehensive account mentioning the applications of ESD has been written by Jaworek [Jaworek 2007] and should be consulted for details.

1.4 Motivation and Introduction of this Thesis

The motivation of this thesis is to introduce and elucidate ESD as a proven method for the processing of functional thin films. Until now ESD has been mainly considered as a tool in spectroscopy and bio-technology. A variation of ESD is Electrohydrodynamic printing where jet is not allowed to break and fine patterns are patterned on the substrates [Choi et al. 2009 & Kim et al.]. However this application is only limited to silver and copper metals pattern deposition. Depositing metal oxides and absorber layers of solar cells via ESD has not been taken yet as a topic and when it is taken only preliminary information has been given without any characterization. Therefore it is very necessary that ESD should be elucidated for its successful use in the fabrication of functional thin films which can be used in different microelectronic and optoelectronic devices. ESD has the following main advantages: (i) applicability to a broad spectrum of materials such as inorganic materials, synthetic polymers, proteins, and DNA; and (ii) the ability to deposit thin polymer films with nano-microscaled structures, which range from spheres to fibers under atmospheric pressure. In addition, the advantage of electrospraying is that the droplets can be extremely small, down to the order of 10's of nanometres, and the charge and size of the droplets can be controlled to some extent be electrical means. Another advantage attached to ESD process is its non-toxicity and environment friendliness as inert inks containing nano-particles dissolved in suitable solvents are used to deposit thin films.

The production of toner powder requires a narrow particle size distribution. If theparticles are too big, then the quality of the printing is too low. If the particles are toosmall, then it is impossible to print them. Also, the toner powder should form a firm layer of particles. This is only possible if the size distribution is sufficiently narrow.

In combustion processes a smooth burning process requires droplets of equal size. However, in this case the low flow rate per spraying point is often a large drawback.

The high droplet charge offers for paint spraying the possibility to guide the droplets to the target. In this way only a small amount of paint is lost. Also, for crop spraying,

the high droplet charge helps to enhance the collection of the droplets on the plants. So less toxic chemicals have to be used, and fewer chemicals come into the environment. Electrohydrodynamic Atomization can also be used to produce thin layers of polymorph material on a surface. The high droplet charge guides the droplet to the surface. The controllable size makes it possible to vary the thickness of the Layer, and to vary the pore size of the layer. The distance between the spraying point and the surface of the counter electrode is an extra parameter that can be used to control the amount of evaporation of the droplets. A monodispersed spray produced in the Cone-Jet mode has also a very narrow charge distribution. So in this mode, the residence time in the air is almost equal for all droplets [Hartman 2006].However the biggest advantage of ESD, where it bears lots of importance and beats its competitors is that the deposition process is carried out at room conditions, the process is very simple and cost effective. No need of the creation of high vacuum and maintaining temperature thereby precluding the need of costly and intricate inter-related vacuum systems and components. Therefore if ESD is successful in making comparable films, then it's a very big achievement and ESD becomes a very strong potential method for functional thin film fabrication, which is the motivation behind this work.

In this work three different functional thin films are demonstrated i.e of Copper Indium diSelenide (CIS), Zinc Oxide and Aluminum doped Zinc Oxide (ZnO:Al). These three layers constitute, in addition to CdS and Mo layer, a solar cell where CIS layer acts the absorber layer, ZnO layer acts as electron injection layer and ZnO:Al layer acts as the window layer. No being pure metal and CdS being very toxic material is very difficult to undergo ESD process, however with further research and developing technology, if these two layers are also deposited viaESd, then we will be able to make completely printed 2^{nd} generation solar cells via ESD. The layers presented in this thesis are completely characterized and hence this demonstration can act as a breakthrough in the field of thin film deposition industry.

The remaining part of this thesis has been divided into 5 chapters where the next chapters gives a complete account on ESD while the next three chapters discuss ink preparation, film deposition and characterization of CIS, ZnO and ZnO:Al respectively. In the end a chapter is dedicated to the Summary of the thesis.

2. Electrospray Deposition Technique

In electrospray deposition, the liquid is pulled out of the nozzle rather than pushed out as in the case of conventional inkjet systems. When the liquid is supplied to nozzle without applying the electric field, a hemispherical meniscus is formed at the nozzle tip due to the surfacetension at the interface between the liquid and air. When the electric field is applied betweenthe liquid and the ground plate (located under the substrate), the ions with same polaritymove and accumulate at surface of the meniscus. Due to ions accumulation, the Maxwellelectrical stresses are induced by the Coulombic repulsion between ions. The surface of theliquid meniscus is mainly subjected to surface tension σ_s, hydrostatic pressure σ_h andelectrostatic pressure σ_e. If the liquid is considered to be a pure conductor, then the electricfield will be perpendicular to the liquid surface and no tangential stress component will beacting on the liquid surface. The liquid bulk will be neutral and the free charges willbe confined in a very thin layer. This situation can be summarized in the following equations.

$$\sigma_h + \sigma_e + \sigma_s \tag{2-1}$$

Since the liquid is not a perfect conductor, the resultant electric stress on the liquid meniscushas two components, i.e. normal and tangential as shown in figure1. This repulsion force(electrostatic force) when exceeds the certain limit deforms the hemispherical meniscus to acone. This phenomenon is known as the cone-jet transition, which refers to the shape of meniscus [Poon 2002].

2.1 Electrospraying Modes

The mode of electrohydrodynamic spraying is the way the liquid is dispersed into droplets, and is characterized by two criteria [Jaworek&Krupa 1999]:

1. The geometrical form of the liquid at the outlet of the capillary (drop, spindle, jet),

2. The mechanism of the disintegration of the jet into droplets (type of instability).

The spraying modes differ significantly in their geometrical form as observed in continuous light. These differences result from the microstructure of the jet, its formation and disintegration into droplets. Usually, each mode commences suddenly at certain voltage and flow rate, and is sustained within a certain interval of their values. Then, it abruptly changes into another mode of spraying. The spraying modes differ significantly in their geometrical form as observed in continuous light. These differences result from the microstructure of the jet, its formation and disintegration into droplets. Usually, each mode commences suddenly at certain voltage and flow rate, and is sustained within a certain interval of their values. Then, it abruptly changes into another mode of spraying.

Dripping mode

The dripping mode of ESD does not differ significantly from the natural dripping i.e. when no applied to the capillary and only flow rate is given. The drops are formed as regular spheres detaching from the capillary as the weight of the drop and the electric force overcome the capillary forces. The exception is that with the voltage increasing the meniscus elongates and the drop becomes smaller.

The similarity extends also to the satellite droplets for liquids of low viscosity. However, for higher voltages, the drop is, for some time, connected with the capillary by a thread, which next breaks off to a few of smaller droplets. After detachment of the drop, the meniscus contracts back forming a hemispherical-like meniscus.

Micro-dripping mode

In micro-dripping mode, liquid at the outlet of a capillary forms a stable meniscus, at the end of which a small, much smaller than the capillary diameter, droplet is formed.

The droplet detaches from the meniscus and no further disintegration takes place. The main difference between dripping mode and micro-dripping mode is that there is no meniscus formation after droplet generation and continuous drop generation depending upon the flow rate and applied voltage. For liquids of low viscosity, this filament breaks off under the electrostatic and inertial forces into smaller droplets. With viscous liquids the broken filament contracts both into meniscus and the detached droplet with no satellite droplets' emission. The size of the droplets can range from a few micrometers up to a few hundred of micrometers in diameters and the droplet size distribution is usually monodispersed. The frequency of the emission of the droplets ranges from a few up to a few thousands of droplets per second.

Spindle mode

In the spindle mode, the meniscus of liquid elongates in the direction of electric field as a thick jet and detaches as a vast spindle-like fragment of liquid. Because of the shape of the jet emitted, this mode is referred to as spindle mode. The spindles, after detachment can disintegrate into numerous smaller droplets of different sizes, hence resulting in poly-dispersed spraying. After the spindle detachment, the meniscus contracts to its initial shape and a new jet start to be formed. The spindle can be sometimes connected with the capillary by a thick thread several mm long. The thread is not linear in its form, but whips irregularly. In the case of low viscosity liquids (ethanol) also a single thin thread can be ejected from the leading side of the spindle, similar to the micro-dripping mode. This thread detaches from the main drop and next disrupts into several small fragments forming siblings or fine poly-dispersed aerosol. The spindle mode differs from the dripping mode in that no regular droplet is ejected from the meniscus but only elongated irregular fragments of liquid. Main droplets are usually different in size, with diameters varying in the range of 300 to 1000 μm [2] while satellite droplets of ~100 μm.

Unstable cone-jet mode

Just between the spindle mode and stable cone-jet mode, occurs the unstable cone-jet mode. This mode occurs when the applied voltage is not good enough to overcome the surface tension forces permanently, but is enough to overcome these forces

temporarily. Hence the jet is not stable and we can have many instances of meniscus recoil. The temporary jet also breaks up and hence disintegrates into many smaller droplets.

Cone-jet mode

In the cone-jet mode, the liquid forms a regular, axisymmetric cone with a thin jet (<100 μm in diameter) at its apex. According to Cloupeau and Prunet-Foch [Cloupeau&Prunet-Foch 1994] the cone can assume three different forms: with linear sides, convex or concave. The jet flows along the capillary axis or deflects from it only on small angle. The jet at its end undergoes varicose [Cloupeau&Prunet-Foch 1989] and kink [Jaworek&Krupa 1992] instabilities.

In the case of varicose instabilities, the waves are generated on the surface of the jet, but the jet does not change its linear position. In the nodes of the wave the liquid contracts and the jet disintegrates into equal droplets, which further flow close to the capillary axis.

In the case of kink instabilities the whole jet moves irregularly off the axis of the capillary, with high amplitude and breaks up into series of fine droplets due to electrical and inertial forces. The aerosol is spread out off the axis, but nearly uniformly in the spray cone of an apex angle of 50-60^{o}. Monodispersed droplets of mean diameter of about 30 μm or smaller are produced within this mode.

Variants of this mode are Oscillating-jet mode and Precession mode and are discussed in [Jaworek&Krupa 1999] in detail.

Multi-jet mode

The reason behind the occurrence of multi-jet mode, where the meniscus becomes flat with small cones at distinct points at the circumference of the capillary, from which fine jets of liquid are ejected, is still unknown. The diameter of the jets, in this mode, is smaller than a few of tens of micrometers. The jets disintegrate due to kink instabilities, into small droplets, forming a fine mist around the capillary. Near the capillary, the aerosol does not fill the whole spray volume but only is dispersed in a

few narrow streams which seem to be located uniformly around the axis. The number of the emission points increases with the voltage increasing.

Apart from dripping mode, each mode of ESD produces atomization. However, the stable cone-jet mode is used for the thin film deposition [Muhammad et al. 2011, Choi et al. 2010, Samarasinghe at al. 2008] because of its mono-dispersed droplet production, very stable atomization process and smooth deposition. A real time depiction of ESD in stable cone-jet mode, as captured by a digital camera is produced in 2.1 below. A very stable and smooth spray stream is visible at the end of the nozzle thereby assuring a smooth and uniform film deposition.

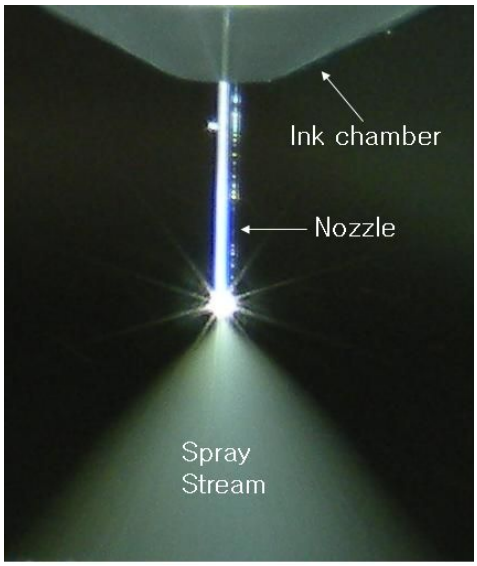

Figure 2-1. Real-time photograph of the spray, emanating from the nozzle. A wide spray stream is clearly visible at the tip of the nozzle.

2.2 Parameters Affecting the Cone-jet

The parameters that influence the formation and transition of stable cone-jet mode can be divided in two groups. Operating parameters i.e. flow-rate, electric field and nozzle diameter, and liquid properties i.e. electric conductivity, viscosity and surface tension [Hartman 2006].

Flow-rate

The flow-rate has a significant effect on the jet diameter and stability of the jet in cone-jet transition. It is the main parameters to control the jet diameter for the patterning process. The flow-rate also affects the applied potential requirement for development of cone-jet (operating envelop) and the resulting the shape of the cone-jet. In electrohydrodynamic jetting, flow-rate also affect the stability of the jet, at low flow-rate the jet is stable, whereas the high flow-rate in cone-jet region destabilize the jet resulting in shorter jet length. This is due to amount of charge carrying at high flow-rate which destabilizes the jet. The typical effects of the flow-rate on stable cone-jet mode are shown in figure 3.

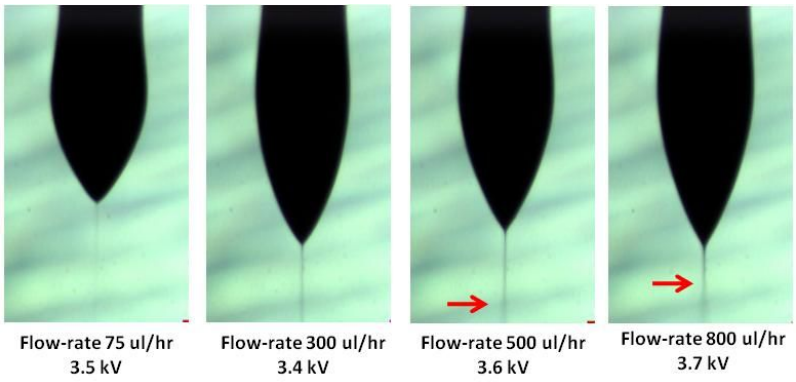

Figure 2-2. Effect of flow rate on the cone-jet transition. The jet diameter increases with increase in flow-rate. The red arrow indicates the jet break-up point.

Electric field (Applied voltage)

Electric field affects the morphology of the cone, by increasing the electric field strength in steady cone-jet mode, the cone-jet recedes towards the nozzle. However, there is less effect on the jet diameter by increasing the applied voltage. At relatively low flow-rate and high electric field, the jet disintegrated into mist of small droplets also known as electrospray atomization, this behavior is used for the thin film deposition of functional material. The typical shape of the come at different applied voltage is shown in figure 3.

Nozzle diameter

Nozzle diameter has significant influence on the operating envelope of the stable cone-jet region. Smaller nozzle diameters extend the lower and higher value of flow-rate limit. The voltage requirement for the cone-jet also decreases with decrease in nozzle diameter for any given liquid.

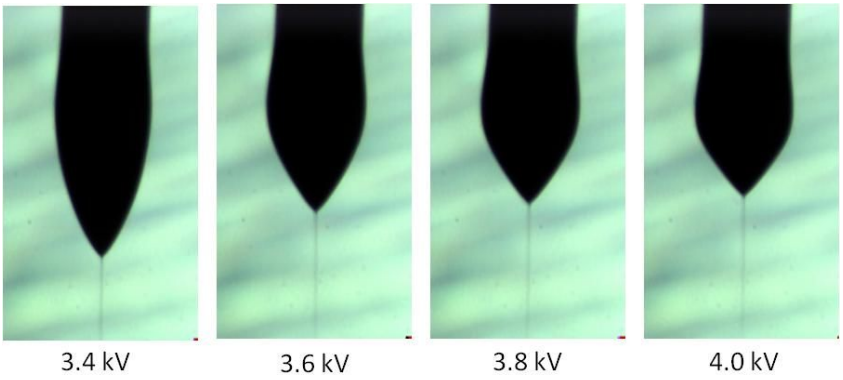

Figure 2-3. Effect of the applied voltage on shape of the cone-jet at constant flow rate (200μl/hr).

Conductivity

The liquid conductivity affects both the shape of the liquid cone and stability of the jet, due to the amount of electric charge on the liquid surface and jet produces is also very unstable because of high radial electric field. Highly conductive liquid deforms into sharp cone-jet shape. Liquid with very low conductivity do not deform into cone-jet by applying electric field, only dripping mode is observed. Liquids with intermediate conductivity range produce steady cone-jet.

Surface Tension

The formation of the jet occurs when the electrical forces overcome the surfacetension at the apex of the meniscus. The required applied voltage will be increased with increase in surface tension of the liquid.

Viscosity

The role viscosity is in the stabilization of the jet and diameter of the jet produced. In high viscous liquid, the jet is stable for larger portion of the length but also produces the thicker diameter. This is due to charge mobility, which is reduced significantly in high viscosity liquid, and causes decrease in conductivity.

2.3 ESD Experimental Setup

The basic experimental setup for the deposition process consisted of following components, as described in the schematic diagram in Figure 2.4 and real time picture in Figure 2.4:

Metallic nozzle (Harvard Apparatus)

Responsible for spray ejection, made of high-quality stainless-steel with inner diameter of 430 µm inner and 610 µm outer diameter.

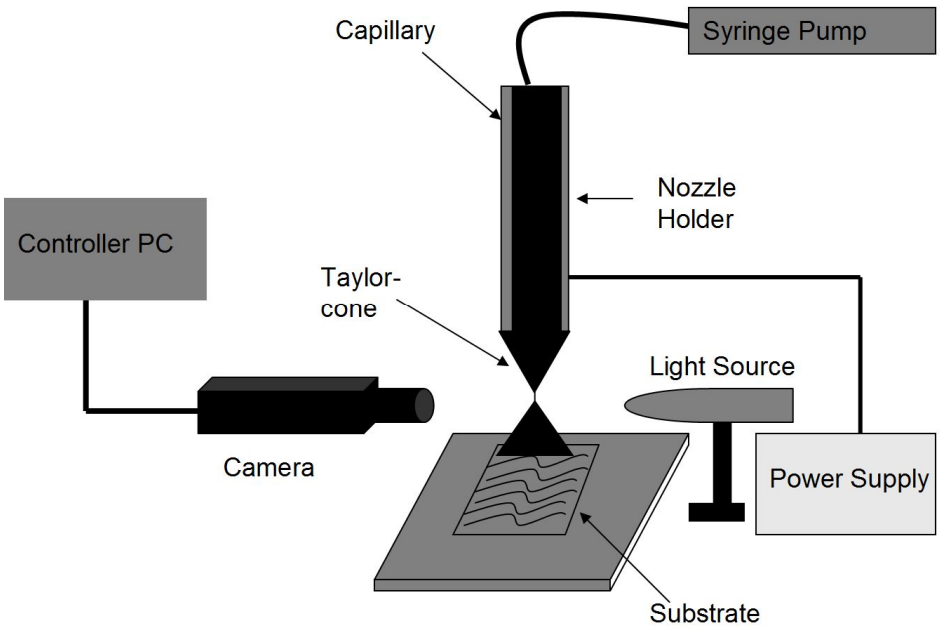

Figure 2-4. Schematic diagram of the system deposition system.

Syringe Pump (Harvard Apparatus, PHD 2000 Infusion)

Connected to the nozzle, the syringe pump maintains the minimum required flow rate for the spray ejection.

Power Source (NanoNC)

A high voltage power source connected between the capillary and copper plate ground electrode generates highly concentrated electric field at the capillary outlet and generates the largely mono-dispersed electrospray of the nano-particles.

Camera (MotionPro X)

A high resolution CCD camera is connected to the main computer and is responsible for the high speed, high resolution capturing of the events going on at the capillary tip i.e. dripping and Taylor- cone formation etc.

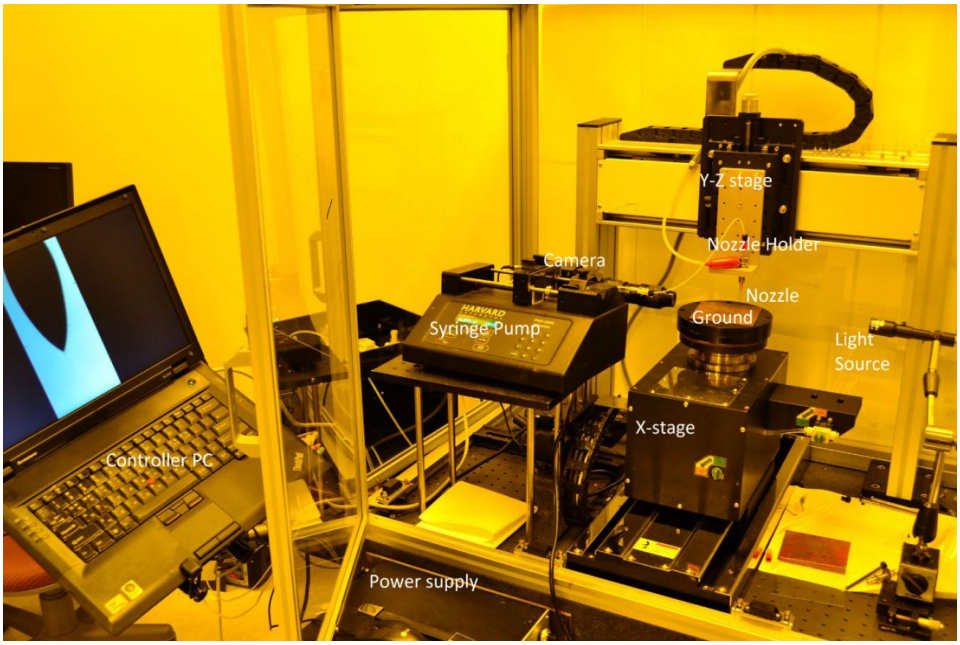

Figure 2-5. Real-time photograph of the deposition system.

Miscellaneous Equipment

Teflon tubing is used for the solution supply from the syringe to the nozzle. Metallic nozzle is mounted on an independent plunk capable of moving in the y and z-direction (vertical and lateral) while the copper plate electrode holding the glass substrate, is attached to the stage which is capable of moving in x direction (linear direction).

3. Deposition of Copper Indium diSelenide Films

The demand of cheap and robust solar cell devices has increased manifolds in the backdrop of the fast evolution and progressing interest in the concept of green energy production. Different generations of solar cell design according to configuration and efficiency are there. Second generation solar cells, comprising primarily of CdTe and $CuInSe_2$ (CIS) or $CuInGaSe_2$ (CIGS) as the absorber layer are more popular research topics than the first and third generation photovoltaics comprising primarily of Silicon based and Organic photovoltaics respectively. In addition to the production of green energy, it also carries the same importance to make the respective device production processes as straightforward as possible. The conventional CIS/CIGS based solar cell fabrication methods usually involve intricate processes like sputtering and chemical or physical vapor deposition methods both involving vacuum and non-vacuum based methods. Vacuum-based processes mainly include sputtering and selenization [Liu et al. 2007, Gupta &Isomura 1998, Titus et al. 2006] and reactive sputtering [He et al. 2003]. Typically, the sputter deposition of a metal-alloy precursor is followed by selenization and sulfurization in reactive H_2Se and H_2 ambient, or recently, by evaporation of a selenium layer on the metal precursor followed by a rapid thermal annealing [Bari et al. 2006]. Non-vacuum-based processes include chemical bath deposition [Sene et al. 2008, Bindu et al. 2003] and coating of nano-particles and deploying them into different deposition mechanisms [Kapur et al. 2003, Eberspacher et al. 2001]. For the purpose of manufacturing CIS based solar cell, nano-particulate copper and indium metal layers of 1–2 μm have been deposited by using Electrospray and selenization together by Kaelin et al [Kaelin et al. 2004]. Another nano-particle based approach for the deposition of CIS films has been suggested by [Yoon et al. 2009]. Electrochemical deposition of CIS layers has been discussed in detail by Savadogo [Savadodo 1998,Sebestian et al. 1999,Hermann et al. 1998].

The advantages of these deposition methods include the growth of layers with precise thickness (~ 1-2 μm) and composition. The achievement of ultra-fine ~1-2

μm thick layers especially for CIS or CIGS using non-vacuum deposition techniques has gathered a lot of research interest. Electrospray deposition is one such technique which has the potential of becoming a reliable and cost-effective technique for the processing of thin CIS films for the use in photovoltaics.

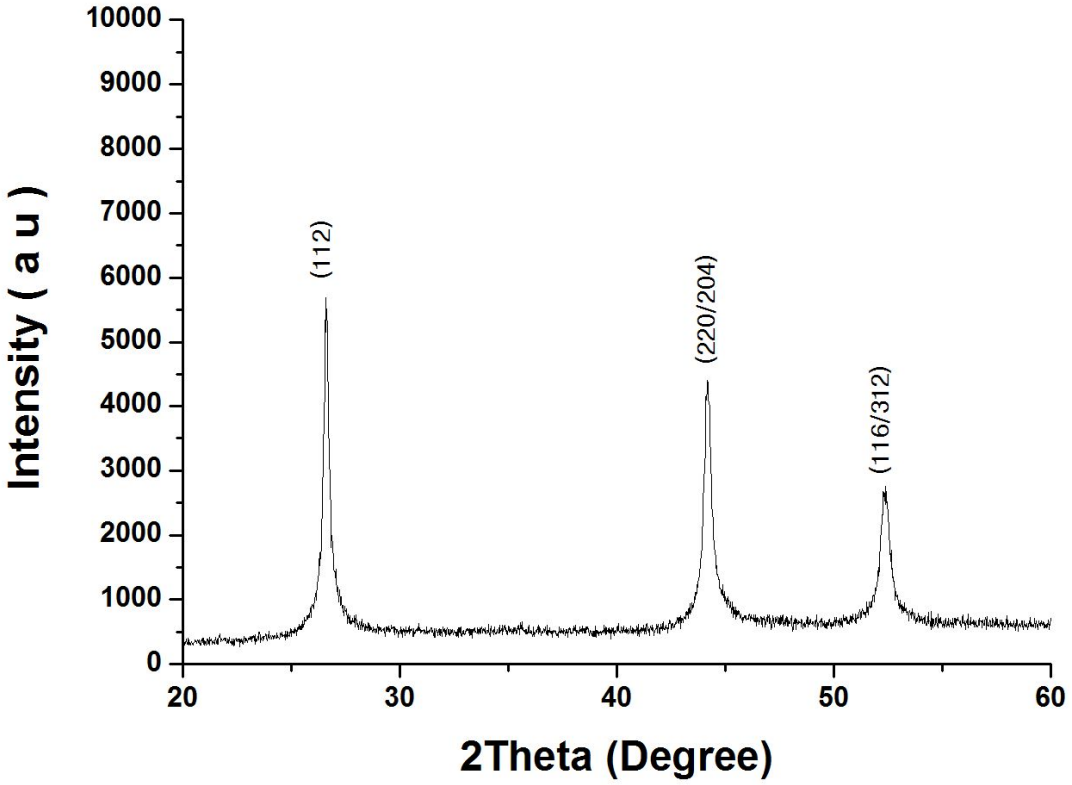

Figure 3-1.XRD representation of the synthesized nano-particle's powder. The chalcopyritestructure is confirmed by the phases marked in the figure.

In this chapter, the electrospray deposition of six different CIS nano-particle ink samples has been investigated. First nano-particles have been manufactured via solvo-thermal process and then they are dissolved in different solvents to make CIS inks. Inks differ on the basis of solvent composition and particle concentration. A combination of Ethanol and Terpineol has been used as the solvent with Polyvinylpyrrolidone (PVP) being used as a non-ionic surfactant. First the optimized solvent composition has been identified using 10 wt% particle concentration[Choi et al.2011] and then particle concentration has been investigated from 7.5% to 15% to get the best particle composition. The deposited layers are characterized on the basis

of their jetting behavior, surface morphology, structural analysis, surface composition, transmittance behavior and electrical characteristics through ESD, scanning electron microscope, XRD analysis, XPS analysis, optical analysis and I-V analysis respectively.

3.1 Materials and Experiment Details

3.1.1 CIS Nano-particle Synthesis

The synthesis of $CuInSe_2$ nano-particles was carried out by a solvo-thermal reaction. In a typical experiment, chalcopyrite $CuInSe_2$ was prepared with 0.04 M of Se powder, 0.02 M of $CuCl_2$ and 0.02 M of $InCl_3$ in ethylene-diamine (ED). The mixture was heated up to 90º C for 30 minutes by totally dissolving the solid, and irradiated with a microwave power of 3 kW at 210º C for one hour to achieve crystallization. The solid product thus obtained was washed with ethanol thoroughly five times and dried in a vacuum oven at 60º C for six hours. For large scale synthesis, a continuous stirred-tank reactor (CSTR) type of microwave system with 3 liter reactor volume was used.

The phase and crystallinity of the samples were determined using an X-ray diffractometer (Rigaku D/MAX IIIB), Fig. 3-1, while the chemical composition of $CuInSe_2$ particles was probed by energy dispersive X-ray spectrometer (EDX), Fig. 3-2a. The stoichiometry of the particles, estimated from the EDX data, was Cu = 0.88, In = 1 *and* Se = 1.98. Average size of the particles, as confirmed by transmission electron microscopy (TEM) came out to be approximately 20 nm, Fig. 3-2b. It is worth mentioning here that the particle size directly influences the grain size in the deposited films, as governed by the Brus equation [Dviwedi et al. 2010].

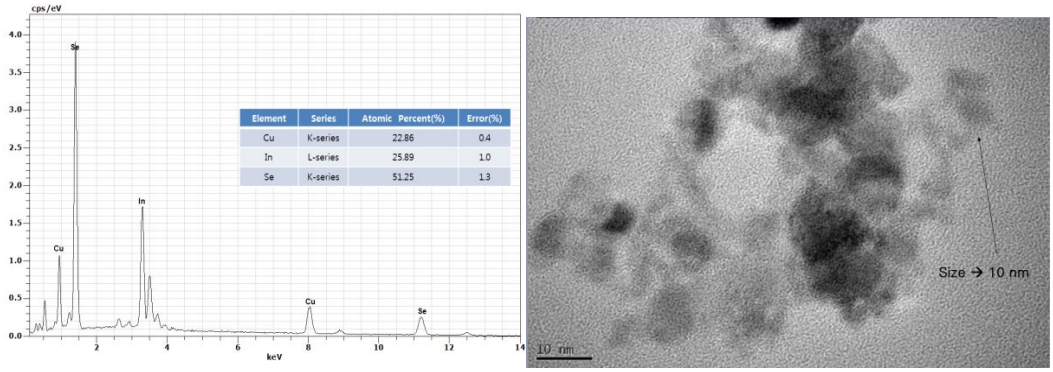

Figure 3-2.a:EDX analysis representation of the synthesized nano-particles. Inset shows the atomic composition and the measurement error.**b:**TEM micrograph of the synthesized nano-particle's powder. Particles of as low as 10 nm are seen.

Non-ionic surfactants, Poly(vinylpyrrolidone)purchased from Aldrich has been used for better dispersion. At first, the solid content was kept at 10wt% and three different solvents were used. First solvent composed of 70% ethanol and 30% Terpineol. Second solvent was composed of 50% ethanol and 50% Terpineol while the third solvent consisted of 30% ethanol and 70% Terpineol. CIS nano particles dispersed in the solvent were ultrasonicated for 5 minutes with pulsed signals at a frequency of 0.4 kW before mixing with PVP and other components. After identifying the optimized solvent concentration to be 50% ethanol and 50% Terpineol (see the results and discussions section of this chapter), 3 more inks, differing in particle wt% (7.5%, 12.5% and 15 %) have been made using this solvent via the same procedure adopted for the first three inks. The stability of the inks has been investigated using Turbiscan MA 2000. The turbi-scans of all the six inks are given in Fig. 3-3. As can be seen for the inks with different solvent compositions, Fig.3-3 (a-c), the dispersion is best in the case of E5T5 (50% ethanol 50% Terpineol) as depicted by balanced transmission peaks at the bottom of the sample holder. However the other two compositions are also satisfactory as far as the dispersion stability is concerned. Figure 1d-1f shows that 12.5 wt% ink as the best of the lot where the transmission loss occurring at the lowest distance and from the view point of the general stability of the analysis. However other two compositions also show satisfactory stability as revealed by their respective turbi-scans.

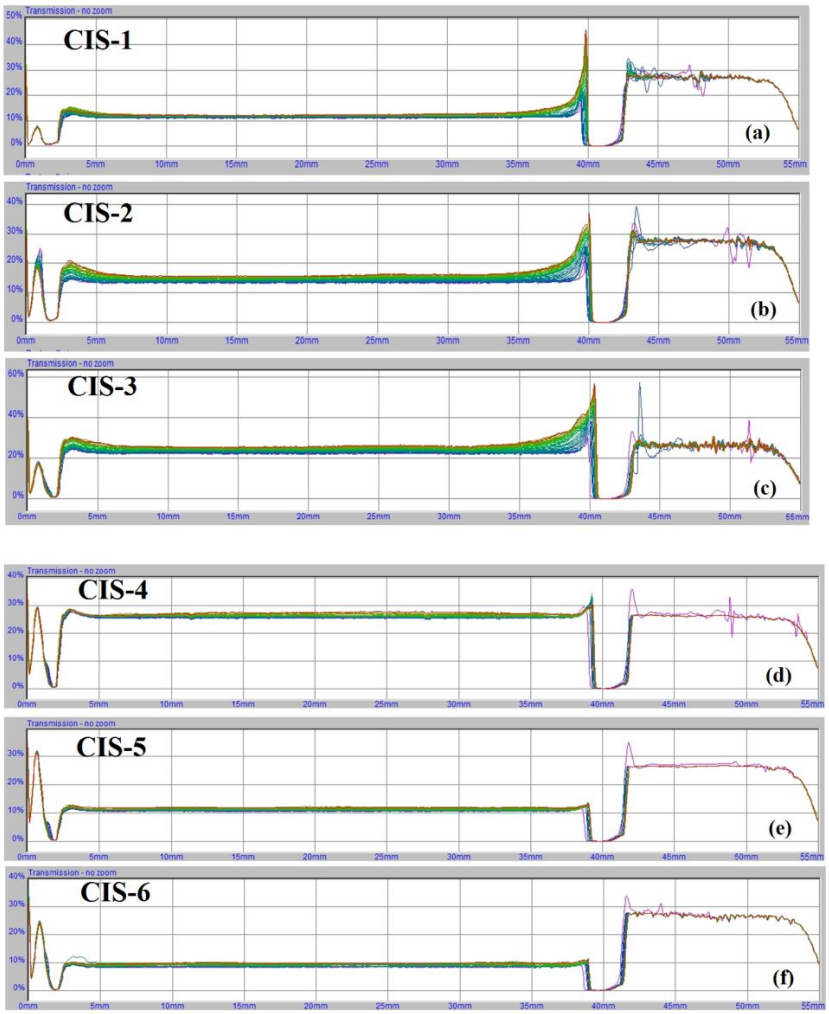

Figure 3-3. Turbi-scans of all the CIS inks showing good stability where CIS-5 shows the best stability of all the inks.

The physical properties of all the inks are given in Table 1. The physical properties of the ink were measured by conductivity and surface tension meter. The measurement of viscosity was carried out with a stain-controlled viscometer for all the measurements. The dielectric constant of the solution was measured using a dielectric constant meter.

Table 3-1. Characteristic properties of CIS inks

Sample	Solvent		Particle wt%	Conductivity (μS/cm)	Surface tension (N/m)	Viscosity (cP)	Dielectric Constant	Density (Kg/m^3)
	Ethanol (%)	Terpineol (%)						
CIS-1	70	30	10	9.8	11.5	1.7	24.6	1130
CIS-2	50	50	10	6.8	17.3	3.5	17.5	1235
CIS-3	30	70	10	1.3	24.7	7.2	11.9	1560
CIS-4	50	50	7.5	7.0	9.9	2.9	19.5	1247
CIS-5	50	50	12.5	7.1	17.3	4.52	21.2	1285
CIS-6	50	50	15	7.2	27.2	4.58	23.4	1298

3.1.2 Film Preparation and Characterization

2cm ×2cm Molybdenum coated glass substrates, obtained from Korea Research Institute of Chemical Technology, has been used as the substrate. Before the deposition process, the substrates were cleaned with acetone and then irradiated with UV light in the UV cleaner for 15 minutes. The electro-sprayed samples were heat treated from the room temperature to 200 ^{o}Cat 0.4 ^{o}C/min and this temperature was maintained for further 2 hours so that all the solvent is evaporated from the layer. The films were then allowed to cool in the furnace itself in off-condition and removed from the furnace after 12 hours. The sintered samples to be analyzed by Field Emission Scanning Electron Microscope (FESEM) were then coated with Platinum in a sputter coater before examination while rest of the samples were stored as it is. The thickness of the deposited films was measured by via ellipsometry. To check the intactness of the chalcopyrite structure of the nano-particles on the film, X-ray diffraction analysis was carried out. Film's compositional analysis was done using X-ray photoelectron spectroscope and optical properties of the films were obtained by UV/VIS/NIR spectrophotometer. Agilent 1500A has been used for the electrical characterization of the films. Aluminum electrodes have been deposited on the films via e-beam sputtering to make the contacts.

3.2. Results and Discussion

3.2.1 Taylor Cone and Spray Formation

The main advantage with the cone-jet mode of the electrospray is the larger mono-dispersity of the sprayed particles which carries a lot of importance when dealing with thin solid films. Therefore the emphasis of this study was to achieve the electrospray of the CIS particles with cone-jet mode. Figure 3-4 (a–f) show the achieved Taylor cones for CIS-1 through CIS-6 respectively at 100 µl/hr flow rate and minimum required voltage for stable cone-jet production. An almost symmetric and largely equilateral triangle is observed emanating from nozzle end in all the cases. The spray is virtually undetected as the spray stream is very minute. As can be seen, there is a hint of spray emanating at the end of the jet and there is little wetting in all of the cases i.e. some of the ink has flown upwards along the walls of the capillary. This behavior is because of the hydrophilicity of the nozzle surface and is highly undesirable as it induces certain instabilities in ESD process and results in

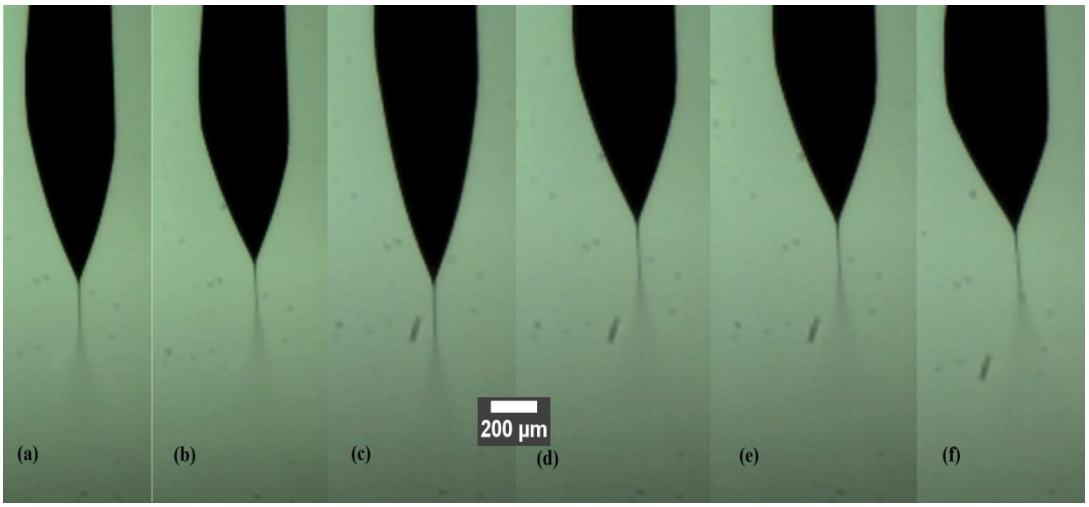

Figure 3-4. Achieved Taylor cones with CIS-1 through CIS-6.

pulsations of the stable cone-jet. However the amount of wetting in this case is not high and can be ignored. All the inks gave good stable cone jets. However a little skewness is visible in the cones for CIS-2, CIS-4, CIS-5 and CIS-6 which occurs if the applied voltage is higher than the required onset voltage. This higher voltage is sometimes required to give stability to the spray process. Taylor-cone for CIS-3 is

biggest of all because of the higher flow rate in this case. Any difference identification from the pictures of Taylor cones is impossible. The difference becomes clear if operating envelops [Choi et al. 2011] are investigated. Certain spraying modes can be identified during ESD and an operating envelope exists where the stable cone-jet mode exists at different flow rates w.r.t. applied potential difference across the nozzle and ground electrode. The first two inks are electro-sprayable from the minimum flow rate of 100 µl/hr to 400 µl/hr while the third ink, rich in Terpineol and having maximum viscosity is not sprayable under 400 µl/hr, Fig. 3-5. All the three inks gave the envelope of 300 µl/hr, that is CIS-1 and CIS-2 were sparyable in stable cone-jet mode from 100µl/hr to 400 µl/hr while CIS-3 gave stable cone jet mode from 400 µl/hr to 700 µl/hr. The analysis was carried out at standoff distance (the distance between capillary outlet and ground) of 12 mm.

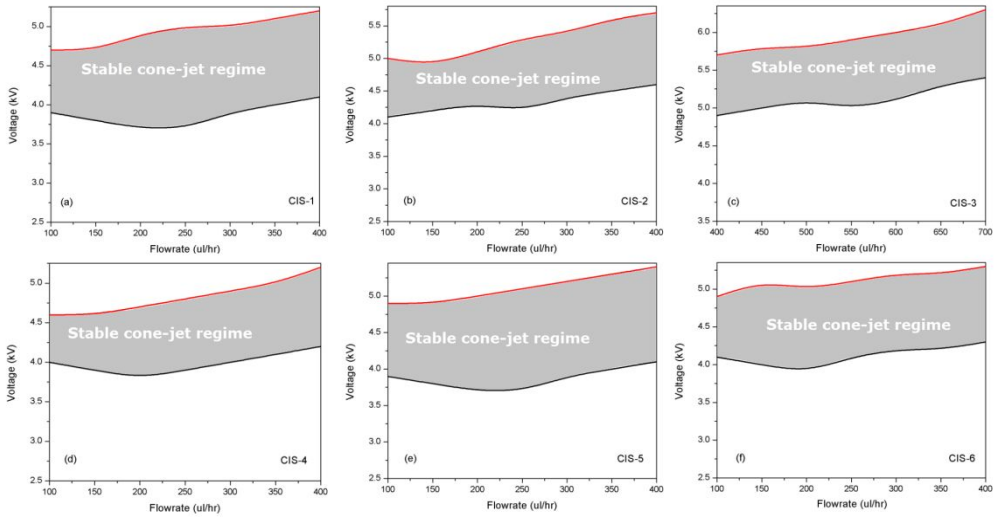

Figure 3-5. Operating envelops of the inks showing stable cone jet regimes at different flow rates and applied voltages.

The voltage requirements increase as the percentage of Terpineol increases in the solvent thereby reducing the dielectric constant of the ink. Therefore for CIS-1 minimum required voltage for stable cone-jet was 3.7 kV at 250 µl/hr, while for CIS-2 it was 4.1 kV at 100 µl/hr. In the case of CIS-3 minimum required voltage was 4.8 kV at 400 µl/hr. If we have a look at the operating envelops of CIS-4, CIS-5 and CIS-6, we see that there is no difference between the flow rate regime and little to no

difference in required voltages, however the operating envelope of CIS-5 is broader than that of the other two inks and required voltage is also lesser in this case. Therefore CIS-5 is the best of the inks. Better ink stability and dispersion and suitable physical properties might be reason of this behavior.

3.2.2 Sprayed Layer Characteristics

Fig. 3-6 shows the SEM micrographs of the CIS layers achieved for CIS-1 through CIS-6 at 200 ul/hr for all the inks at respective voltage according to Fig. 3-5, except CIS-3 where 500 ul/hr has been used. Standoff distance of 10mm with substrate speed 1 mm/s is used for all the inks except for 20mm with 5 mm/s for CIS-3. Higher standoff is used for CIS-3 because of the higher viscosity of the inks, jet length for this case is higher and if distance smaller than this is used we wont get any spray but a continuous pattern will be deposited [Poon 2002]. Also higher substrate speed is used since at higher flow rates, if the substrate speed will be small, the layer deposited will be very thick. So to eliminate this problem a higher substrate speed is used.

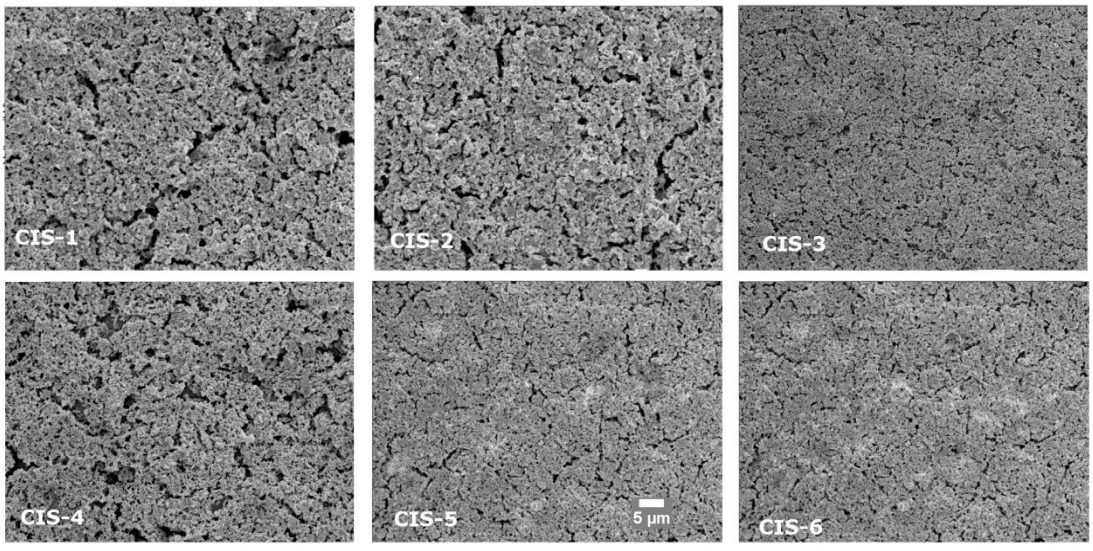

Figure 3-6.SEM micrographs of the layers produced via CIS-1 through CIS-6. Exceptional layer quality is achieved with CIS-3, CIS-5 and CIS-6.

Good particle integrity is obtained and particles are flocked together into agglomerates penetrating into each other. However some pores are also observed apart from the recrystallization of CIS layer in almost all the layers. The isolated sintering of a group of particles is also observed. Between CIS-1 to CIS-3, layers with CIS-2 are the best one if surface morphology and thickness both are considered. The highly porous nature of CIS-1 layers is because of high ethanol concentration which evaporates at low temperatures. As the ethanol concentration decreases and Terpineol concentration increases, layer morphology improves as in the case of CIS-2 and CIS-3. CIS-3 presents best layer morphology of the three films because of very high flow rate but layer thickness is on the higher side. Therefore we pick CIS-2 with 1:1 (Ethanol:Terpineol) solvent as the best solvent. Layers for CIS-3, CIS-5 and CIS-6 are exceptional as compared to other three inks where cracks are and pores are of much bigger extent. If CIS-2, CIS-4, CIS-5 and CIS-6 are compared then it can be easily deduced that as the particle concentration increases, the layers becomes more condensed and uniform. Therefore CIS-6 presents best of the layers with CIS-5 and CIS-6 do not differ much. Hence CIS-5 and CIS-6 are the pick of the inks if the surface morphology is concerned. The main advantage of electrospray lies in the fact that the deposition process is very simple and is carried out at room temperature. Achievement of the presented results at room conditions and open environment is an achievement and it is believed that ESD can be a good alternative deposition process for manufacture of solar cells.

3.2.3 Layer Thickness

Figure 3-7 provides the thickness measurement results of the films achieved by CIS-1 through CIS-6 respectively. The thickness was checked at 10 different places on the film. The results obtained here should not be accounted for the surface roughness of the film, as the instrument actually focuses on a large area rather than a point and gives the numerically calculated average thickness value in the whole focused area. As can be seen layers deposited using CIS-3 are very thick and make it un-usable for practical applications. While layers with CIS-1 are quite thin but there porosity rules them out as well. If we compare layers with CIS-2, CIS-4, CIS-5 and CIS-6, we will

see that layer thickness increases as the particle concentration increases.

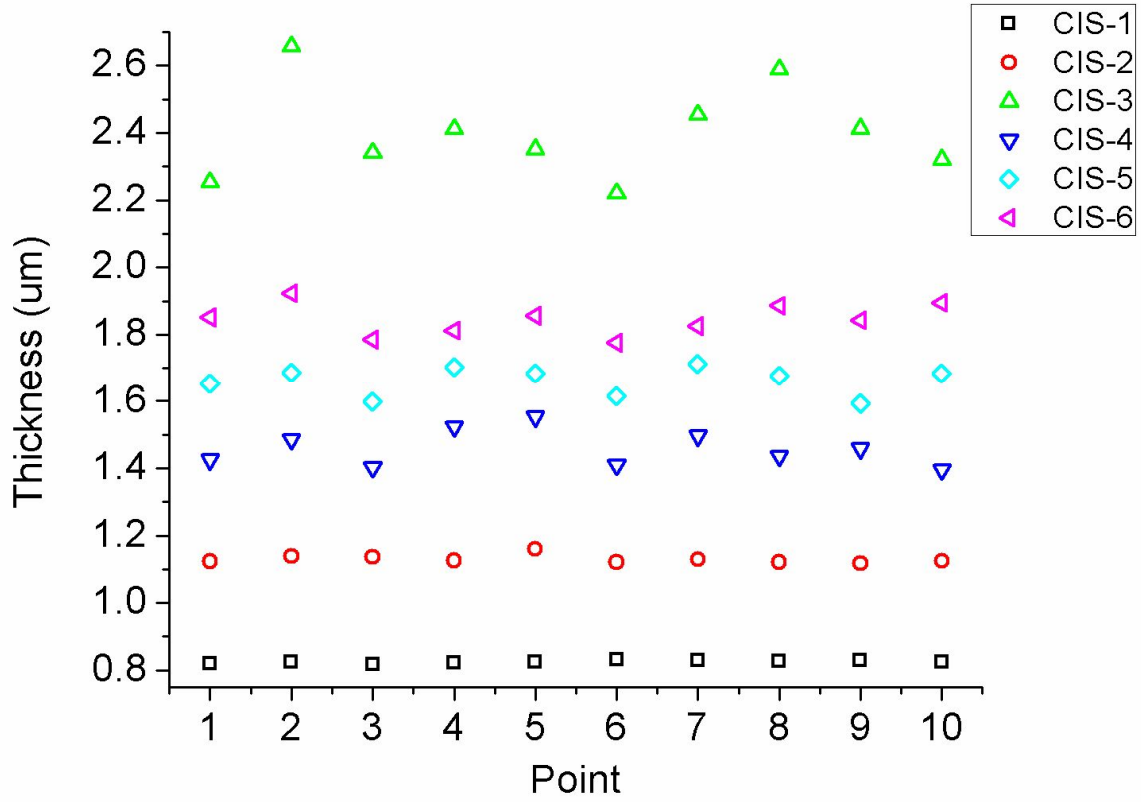

Figure 3-7. Thickness profile of the films at 10 different points on each film. Thickness is calculated using ellipsometry technique.

Although all these inks gave required thickness, if we take into account layer morphology from the previous section we see that 12.5 wt% ink is the best of the lot as it gives good ~1.6 μm thickness with good layer morphology. An anomaly can be pointed out that CIS-1 with 10 wt% particle concentration produced layer with lesser thickness than that with CIS-4 with 7.5 wt% particle concentration. Here the importance of a suitable solvent comes into picture as in the case of CIS-1 where 70 ethanol is present in solvent evaporated very quickly and mostly the nano-particles only were deposited on the substrates while in the case of CIS-4, higher amounts of Terpineol allowed the particles to settle better in the film and stayed for longer times thereby producing thicker layers.

3.2.4 Structural Analysis

The chalcopyrite structure of the deposited thin films of CIS nano-particles deposited was confirmed by X-ray diffraction. The resultant XRD patterns in Fig. 3-8 of layers for CIS-1 through CIS-6 were consistent with the reported data (ICDD card No. 89-5649). In addition to CIS peaks, peaks of Mo substrate layer and that of $MoSe_2$ interface layer between CIS and Mo are visible as well which are according to the reported data [Abou-Rasa et al. 2005, Schmid et al. 1996].

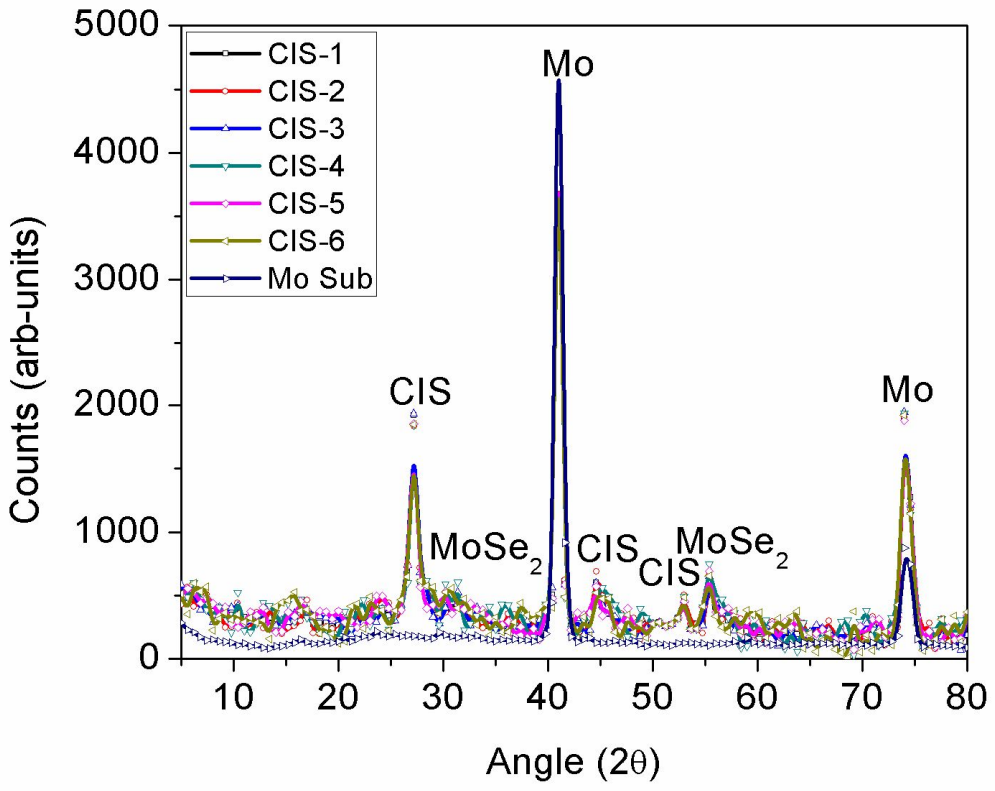

Figure 3-8.XRD analysis representation of the deposited layers. Chalcopyrite structure of the films is confirmed whereas presence of this $MoSe_2$ layer is also verified by its respective peaks. Mo peaks belong to Mo coated glass substrate.

3.2.5 Surface Composition Analysis

To confirm the purity of the deposited films, XPS analysis has been carried out. Figure 3-9 represents the XPS analysis results of the films, deposited on highly doped conducting Si substrate for the layers deposited by inks CIS-1 through CIS-6. The Cu, In and Se peaks are visible according to their sensitivity parameters thereby proving the intact nature of CIS film. Although all the layers exhibit some percentage of carbon, yet the difference becomes clear if a high resolution scan is carried out in the region of carbon peaks, as presented in the inset of Fig. 3-9.

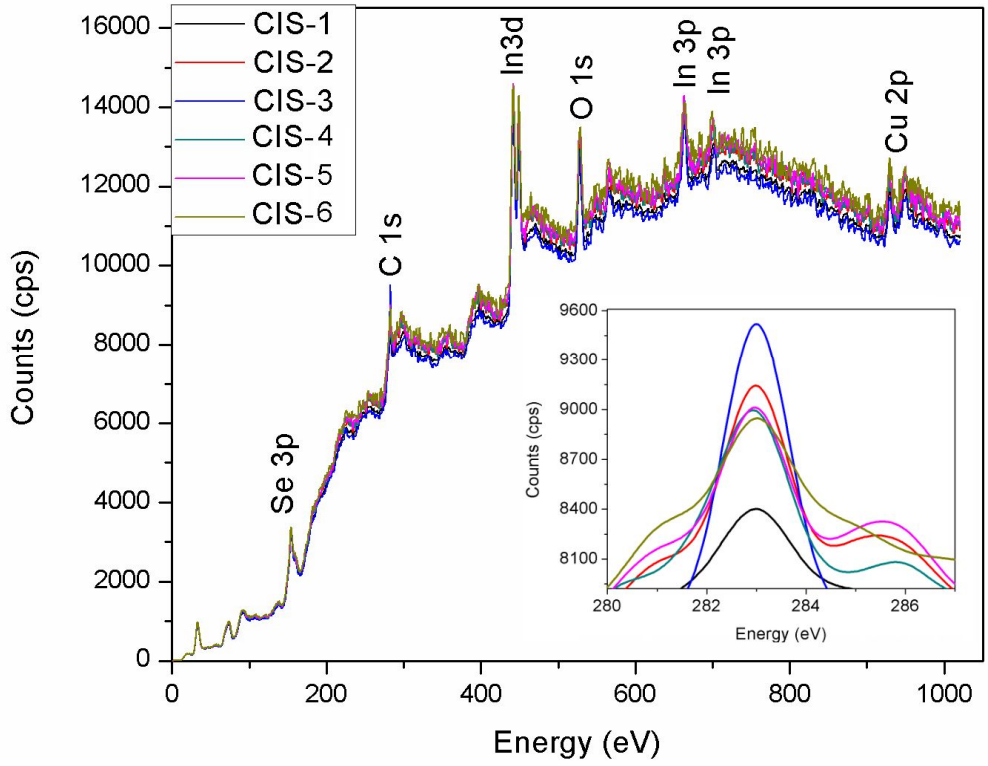

Figure 3-9.XPS analysis representation of the deposited layers. Pure layers are identified with presence of trace amounts of Carbon. Inset shows that Carbon concentration increases when amount of Terpineol increases in the solvent.

Carbon percentage is the highest in the layers deposited via CIS-3 and lowest in CIS-1, while its presence is in the intermediate range for all the inks containing 1:1 (Ethanol:Terpineol) solvent formation. Therefore it can be concluded that the higher the amount of Terpineol in the solvent, higher percentage of carbon will be there. This is because of high boiling point of Terpineol hence making it difficult to evaporate from the films thereby leaving some trace amounts of carbon.

3.2.6 Optical Properties

Figure 3-10 shows the transmittance spectra of the electrospray deposited films for CIS-1 through CIS-6 in ultra-violet (UV), visible and near-infra-red (NIR) spectrum. The transmittance in the UV region for all the films is close to zero, however since major interest lies in the visible region, therefore looking a bit closer reveals that transmittance for films with higher particle concentration is much smaller than that with lower particle concentration, Fig. 3-11. Main reason for this behavior is porosity and thickness of the film. Since CIS-1 and CIS-4 suffer with higher porosity and have relatively less thickness therefore these films exhibit more than 30% average transmittance in the visible region. Layers for CIS-2 also exhibit mediocre performance where average transmittance is around 25%. Layers for CIS-3, CIS-5 and CIS-6 exhibit very good transmittance performance where average transmittance in visible region is just 10% meaning that these layers absorb 90% of the light they receive.

3.2.7 Electrical Characterization

Electrical characterization results of the films produced via CIS-1 through CIS-6 are presented in Fig. 11. All the layers exhibited linear I-V relationship at low voltages however non-linearity increases as the voltage increases and a good over-all semiconductor behavior is exhibited by the films. As clear from the figure, the higher the particle concentration better is the performance of the films. Therefore CIS-4 with 7.5 wt% had the highest sheet resistivity while CIS-6 with 15 wt% had the best sheet resistivity of all the layers. However the electrical performance of the layers

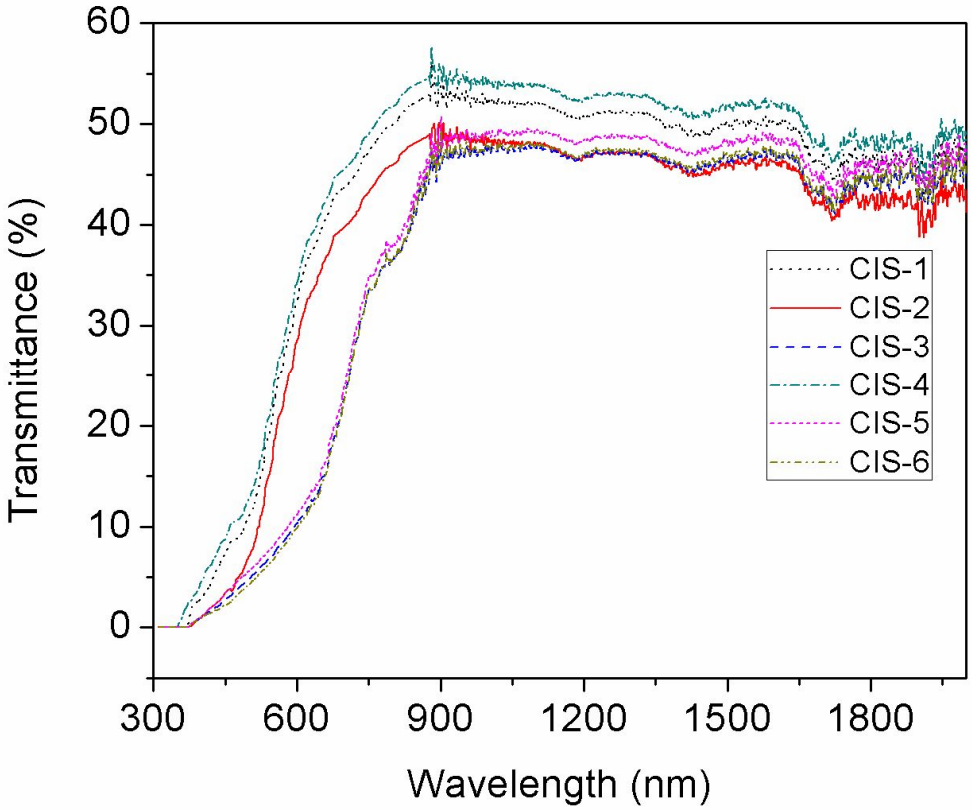

Figure 3-10. Transmittance spectra with respect to wavelength (nm) of incident light in UV, visible and near-infra-red spectrum. An adequate performance has been observed for films.

with CIS-5 matched the performance of that of CIS-6 as well so keeping in view other parameters, CIS-5 is most suited for the use in the fabrication of solar cells with 12.5 wt% particle concentration. Approximate Sheet resistivities of the layers were 58 Ω.cm, 54 Ω.cm, 55 Ω.cm, 76 Ω.cm, 40 Ω.cm and 33 Ω.cm for the layer deposited with inks via CIS-1 through CIS-6 respectively. These values are completely in line with solar cell requirements [Javed 2007, Guillen&Herrero 1992]. An interesting observation here is that layers with CIS-3, having same morphology as the layers with CIS-5 and CIS-6 did not match the electrical performance. This is mainly because the layers are thick and also because of the presence of higher amounts of carbon in these films.

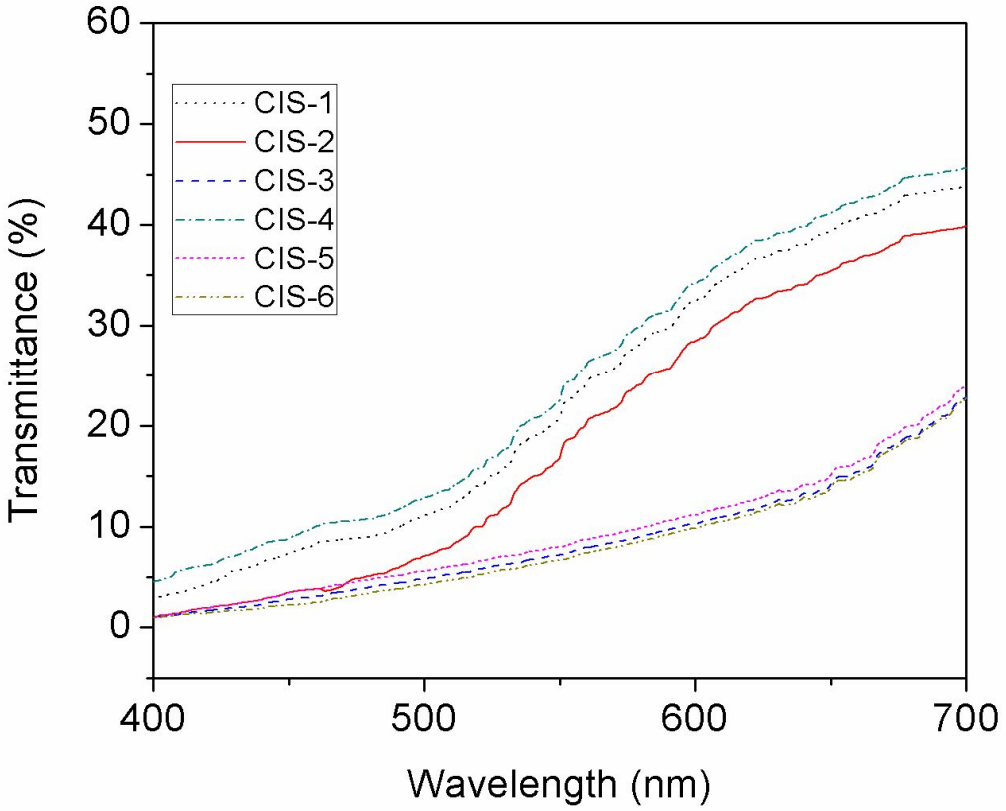

Figure 3-11. Transmittance spectra of the films in visible region, less than 10% transmittance is observed for films with CIS-3, CIS-5 and CIS-6. Mediocre performance is observed for other layers.

3.2.8 Effect of Stand-off Distance

An important parameter affecting the spray characteristics in the ESD process is the distance from nozzle tip to the substrate, known as the standoff distance. The spray profile achieved consisted of a striking behavior of dual-region spray profile as shown in Fig. 3-13a. The whole spray area can be divided into two distinct regions with mildly diffused interface between the two, one with a very concentrated spray (dark white region) and the other with a mild region starting from the end of concentrated spray circumference to the extreme circumference of the spray disk. These two regions tend to vary when the standoff distance is varied. The reason for this dual-region is partly the fact that the spray spurt consists of satellite droplets which are characteristic of the electrospray process. These satellite droplets are lighter and consist of less concentrated particles and are usually at the spray

periphery where the velocity profile is flat, as compared to the main concentrated spray droplets which are bigger and occupy the center region with a mostly parabolic velocity profile. Another reason explaining this behavior is that the spray stream ejected at the cone tip can possibly have a swirl type motion around its axis [Ishikawa &Tsujimura 1998, Chung &Troutt 1988].

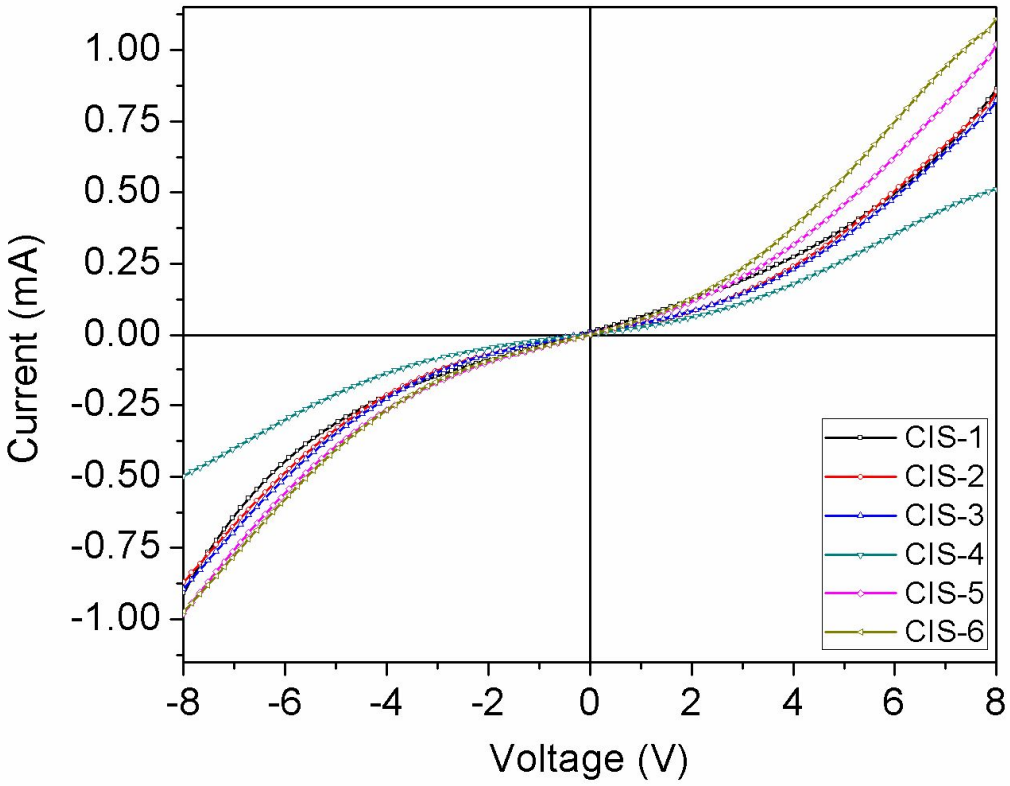

Figure 3-12.I-V analysis results of the films. Layers deposited using inks with higher particle concentration show superior electrical performance over those with less particle concentration.

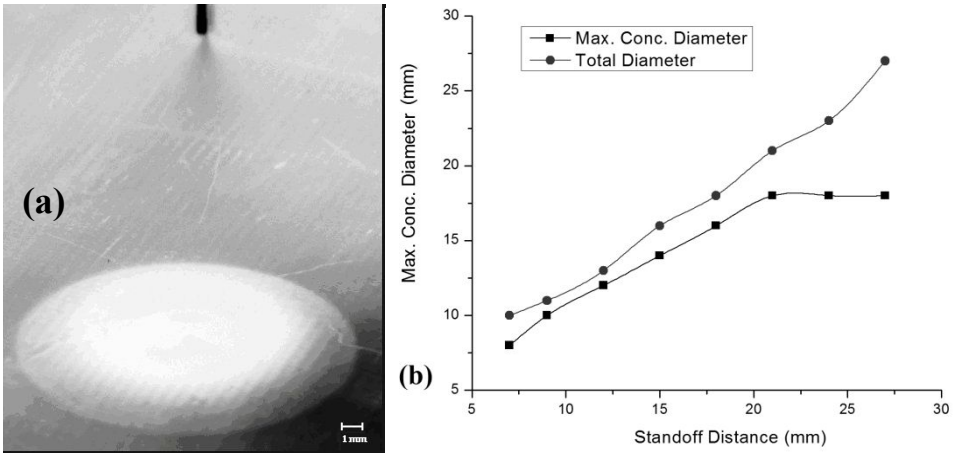

Figure 3-13.a: Photograph showing dual-region spray deposition profile**b:**Variation in the diameters of two regions at different standoff distances.

The presence of tangential electrical forces also supports this theory. As a result, centrifugal forces arise thereby clustering the central region with heavier, more concentrated CIS nano-particles while the lighter part, mostly the solvent is pushed towards the periphery of the deposited layer. Although this explanation satisfies the dual-region behavior, yet further research is required into this matter.

Figure 3-13a gives a glimpse of the two regions deposited by ink CIS-5 at different standoff distances. At a small distance, the concentration of the spray area is largely uniform. However, the mild region tends to increase as the nozzle tip is moved father from the substrate. This behavior again supports the explanation given for dual-region behavior as when the tip is very close to the substrate, there will not be enough flight time for the spray stream to orient in the two regions and hence the concentration difference between the two regions is very small. Inverse estimation techniques can be used to estimate the concentration distribution and is an interesting area of research when deployed for electrospray applications. At a certain threshold distance, the concentrated area diameter gets constant and the mild area goes on increasing. The results given in the previous section were taken at a distance of 15 mm from nozzle tip to substrate. Since the applied voltage and flow rate are the same at each marked distance, the spray layer thickness would vary at different nozzle heights relative to the substrate, i.e. the layer thickness will increase as the distance decreases and vice versa. An important point which comes to mind at this

point is that a spray diameter of 1.5 cm gives a spray area of just 1.76 cm^2, which is small when viewed from the perspective of bulk manufacturing. The answer to this is multi-nozzle spray deposition in which hundreds of nozzles are embedded in the system.

The multi-nozzle setup also takes care of the dual spray region phenomenon as the mild regions of two adjacent nozzles will overlap (being at the periphery) and hence the concentration will double in the overlapping edge region thereby mitigating the drawback of dual spray region as well. The microstructure essentially will remain the same and the layer will be more uniform in thickness and concentration, hence viable for bulk manufacturing of solar cells.

4. Deposition of Zinc Oxide films

Zinc oxide (ZnO) is a wide band gap material and because of its appealing properties like low-cost, non-toxicity, easy availability and high inertness in reduction environments, it has received tremendous attention for its use in many exciting applications. In solar cells, it can be used as window material; can act as a buffer layer or active layer and electrode as well [Matsubara et al. 2003, Bjorkman et al. 2003]. Also it is extensively being used in UV emitters, thin film transistors, liquid crystal displays, gas sensors and other plenty of applications [Oh at al. 2005, Wager 2003, Heo et al. 2004, Wang et al. 2005]. ZnO is also fast finding its applicability in replacing more expensive Indium Tin Oxide (ITO) because of its 1000 times more abundance in earth crust as compared to that of ITO [Song 2008]. Most printable semiconductors today are p-type and available n-type semiconductors have mobility less than 10^{-2} cm^2 V^{-1} s^{-1} which is generally considered to be low for most printed electronic applications [Volkman et al. 2004]. Additionally many printable semiconductors, including organics and chalcogenides are toxic, and their integration into disposable circuits is problematic. Therefore ZnO offers a great avenue to explore for its application as alternative material to many conventional semi-conductors.

As far as the deposition processes for thin films of ZnO are concerned, many conventional processes are available, for example physical and chemical vapor deposition, magnetron sputtering, spin-coating, vacuum arc plasma evaporation, ionic layer absorption and reaction (SILAR), atomic layer deposition, molecular beam epitaxy and sol-gel process to name a few [Wilhelm 2004, Yee et al. 1996, Craciun et al.1994, Natsume et al. 1995, Norris et al. 2003, Ogata et al. 2000, Kumar et al. 2008, Minami et al. 2003, Libera et al. 2008], with each having its own unique advantages and disadvantages. All of these processes are mature enough to deposit high quality ZnO films, however they suffer from certain limitations like controlled environment requirements, complex and invasive process and high processing costs for sophisticated and expensive vacuum systems for some of these processes [Mitzi

2009, Kaelin et al. 2008]. Therefore any process which is able to mitigate these limitations and is still able to produce high quality ZnO layers is of particular interest as an alternative to conventional deposition techniques.

ESD is the technique which has the potential of becoming a reliable, cost-effective and robust technique for the processing of thin ZnO films. Jaworek et al. [Jaworek et al. 2008] used ESD phenomenon to form metal oxide coatings on micro-fibers. In their study they used ZnO as well but their primary concern was only the coating quality. Choi et al. [Choi et al. 2010] and Ding et al. [Ding et al. 2009] in their respective studies have discussed deposition of ZnO through electrospray but the former mainly focused on the physical aspects of ZnO nano-particle ink like contact angle etc and only the surface morphology was discussed while the latter deployed ESD in conjunction with the sol-gel method to deposit the ZnO layers.

The present chapter discusses a comprehensive description of ZnO film formation and assessment right from nano-particles alcosol preparation to film deposition through ESD and its characterization. The layers crystal structure is confirmed through x-ray diffraction (XRD) analysis while the compositional quantification has been carried out using the x-ray photoelectron spectroscopy (XPS) analysis. Surface morphology is characterized through the scanning electron microscope (SEM) analysis and thickness measurements are performed deploying a non-invasive thickness measurement system which is based on the principle of constructive and destructive interference in the spectrum of white light incident on the surface of the film. Finally the electrical properties of the film are tested to verify the fitness of deposited ZnO films to be used in electronic devices and optical characterization of the films is obtained by a UV/VIS/NIR spectrophotometer.

4.1. Experimental Details

4.1.1 ZnO Alcosol Ink Preparation

ZnO nanoparticles were obtained from Sigma-Aldrich and were used as received. Non-ionic surfactant, Triton X-100 (Sigma-Aldrich) was used as a wetting agent for better dispersion of ZnO particles.The solid content was kept at7 wt.%. ZnO nanoparticles dispersed in 99.9 % pure ethanol (OCI Company Ltd.) were sonicated

for five minutes with pulsed signals at a frequency of 0.4 kHz before mixing with 0.01% Triton X-100. The solution was then stirred for 4 hours at 70 ^{o}C using a magnetic stirrer. The conductivity and surface tension of the ink were measured to be 9.85 mS/m and 0.0355 N/m respectively. The density of the alcosol solution was 1150 kg/m^3. In addition, the measurement of viscosity was carried out with a stain-controlled rheometer. A cone-plate fixture of the gap angle = 0.0398 rad and diameter = 50 mm was usedat shear rate ($\dot{\gamma}$) from 1 s^{-1} to 10^3s^{-1} and viscosity was recorded as 0.0128 Ns/m^2.

The films were deposited on glass substrates (Corning 7059) through ESD at room conditions at a substrate speed of 0.25 mm/sec and at a distance of 7 mm between the capillary and the substrate. Before the deposition process, the substrate was rinsed with acetone and then irradiated with UV light in the UV cleaner for 15 minutes. The deposited films were sintered at 500 ^{o}C for 3 hours before the characterization process. A scanning electron microscope (SEM), Jeol JSM-7600F, was used to characterize the surface quality of the deposited films. Film thickness was measured by a state of the art, non-destructive, thin film thickness measurement system K-MAC ST4000-DLX based on the principle of constructive and destructive interference in the spectrum of white light incident on the surface of the film. The crystal structure of the films was verified by x-ray diffraction (XRD) measurements carried out by using Rigaku D/MAX 2200H, Bede Model 200 system. Cu-Kα radiation (λ = 1.054 nm), from the X-ray generator operating at 40 kV at 30 mA was used to record the X-ray diffraction patterns. A scan resolution of 0.2^{o} was used for the measurements and diffraction intensity was recorded in the 2θ range 0 – 80^{o}. The X-ray photoelectron spectroscopy (XPS) analysis of the deposited thin film has been carried out using VG Microtech XPS analysis equipment using Mg-Kα radiation from an X-ray source operating at 12 kV, 15 mA. The survey spectrum was taken at a pass energy of 50 eV, providing an instrumental resolution of 1 eV. The current-voltage (I-V) characteristic curve of the deposited films was measured by Agilent B1500A Semiconductor Device Analyzer. Measurements were carried out with a hold time of 2 seconds and the scan resolution of 30 mV. Finally the transmittance spectrum of the deposited films has been obtained by using the Shimadzu UV-3150

UV/VIS/NIR spectrophotometer in the range of 250 nm to 1100 nm covering the ultraviolet, visible and near-infrared regions.

4.2. Results and Discussion

4.2.1 Taylor Cone and Spray Formation

The ZnO alcosol solution remained stable during the experiments and no sedimentation or disintegration between the solute and the solvent was witnessed at any point on standing for periods of time much longer than the experimental durations. The ESD experiments were initially performed with flow rates varying from 25 µl/hr to 175 µl/hr in order to determine the optimum spraying conditions with the stand-off distance fixed at 7mm. At each flow rate step, applying different magnitude of voltage gives a different mode of atomization and hence various modes were observed such as dripping, micro-dripping, unstable cone-jet, stable cone-jet and multi-jet. Figure 4-1 provides the observed operating envelope of the ZnO alcosol ink representing different atomization modes with varying flow rates and corresponding applied voltages. A stable cone-jet region is shaded to emphasize upon the possible flow-rate and voltage combination for optimized atomization conditions.

Figure 4-2 represents high zoom and high speed images of different atomization modes as achieved at 100 µl/hr flow rate when different voltages were applied. At zero voltage, dripping mode was observed. When the voltage was gradually increased from zero up to 2.9 kV, only micro-dripping occurred. At 3.5 kV, pulsating cone-jet mode was observed. When the voltage was raised to 4.5 kV, stable cone-jet mode and when increased further to 6.0 kV, multi-jetting was observed. If the applied voltage was increased further the jet discharged. A flow rate of 100µl/hr was used throughout the experiments for the deposition of ZnO films. This value was selected as the droplet size is directly proportional to the cube root of flow rate [Ganan-Calvoet al.1997]. However, if the flow rate was too low, the stable cone-jet mode was regularly disturbed or the jet was not stable for a sufficient time span to enable film fabrication.

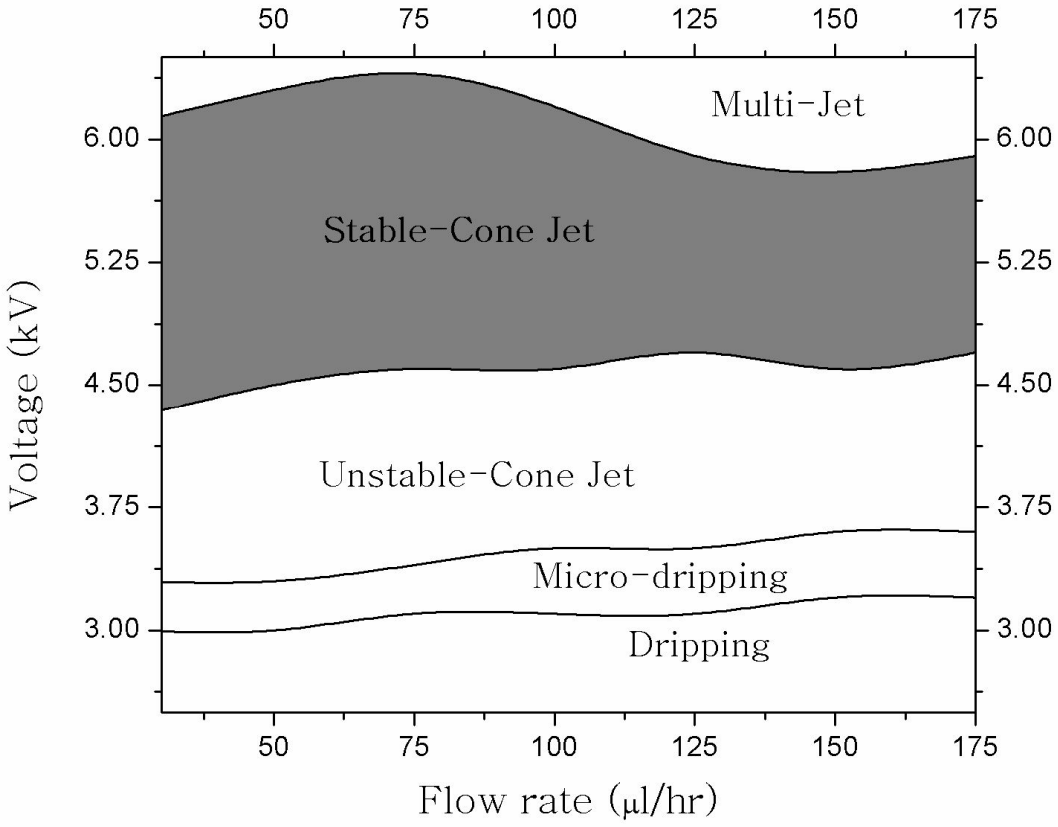

Figure 4-1. Operating envelope representation for different electrospray regimes. The stable cone-jet region is shaded to emphasize upon the possible flow-rate and voltage combination for optimized atomization conditions (Air-gap = 7mm).

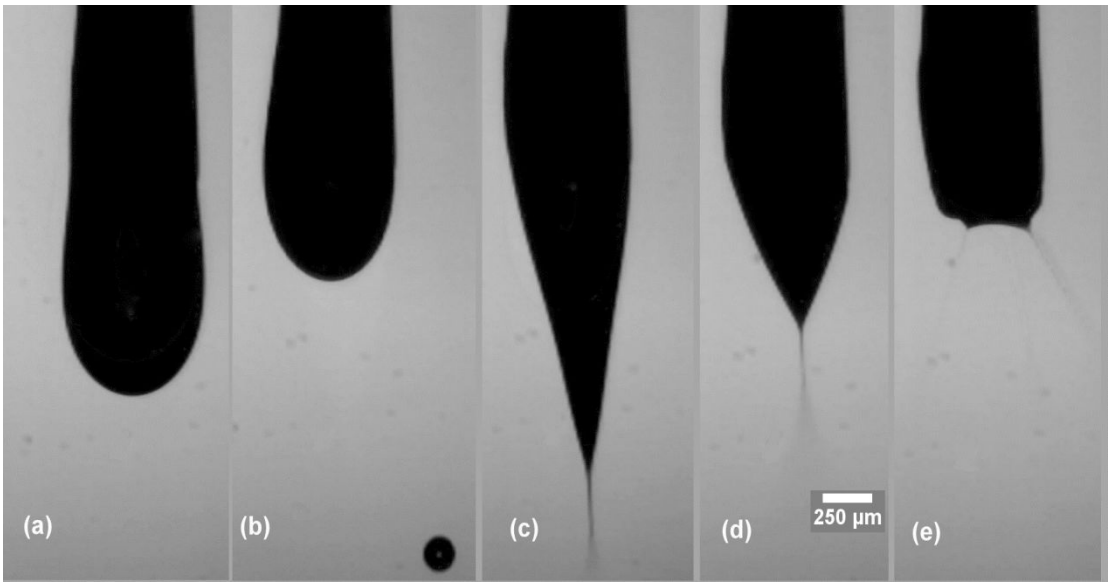

Figure 4-2. Electrohydrodynamic modes observed during the deposition process. a) dripping mode, b) micro-dripping, c) unstable cone-jet mode, d) stable cone-jet mode and e) multi-jet mode.

The occurrence of the classical hydrodynamic atomization requires thehydrodynamic time $T_h$to exceed the charge relaxation time T_q. The two quantities are given as [Ganan-Calvoet al.1997]:

$$T_h = \frac{LD^2}{Q} \tag{4-1}$$

$$T_q = \frac{\varepsilon_0 \varepsilon_r}{K} \tag{4-2}$$

Where, L denotes the axial length of the jet, D is the jet diameter, Q is the flow rate and K is the electrical conductivity. Using the following values for these quantities,

$L = 220\,\mu m$
$D = 22\,\mu m$
$Q = 100\,\mu l/hr = 2.778\times10^{-11}\,m^3 s^{-1}$
$\varepsilon_r = 25$ (For ethanol)
$\varepsilon_0 = 8.85?\ 0^{-12}\ \mathrm{Fm}^{-1}$
$K = 0.00985\ S\mathrm{m}^{-1}$

Implies that $T_h = 0.0038$ seconds which is much greater than $T_e = 2.246 \times 10^{-8}$ seconds. Thus, the required condition for classical electrohydrodynamic atomization is satisfied.

4.2.2 Surface Characterization

Figure 4-3 shows the SEM micrographs of the deposited film. Figure 4-3a represents a low magnification SEM image thereby representing the bulk of the deposited film. As can be seen, the film is uniform, non-porous and smooth. A few hillocks (small hills where ZnO particles make hill-type morphology and rise above the film) can also be seen which form because of the preferential landing of droplets on the substrate [Chen et al. 1996]. This behavior is the characteristic of ESD. Due to the presence of strong electric field created between the nozzle and the substrate, induced charges exist on the substrate which is oppositely charged to that of droplets or the capillary. The charge distribution on the surface is not uniform and mainly depends on the position relative to the nozzle and on the local curvature of the surface. The charges accumulate preferentially where the curvature is more and therefore electric field is concentrated as compared to other substrate areas. Hence when a charged droplet reaches the substrate, it will be attracted more towards these areas and hence a hillock will be created [Chen &Schhonman 2004]. Figure 4-3b and 4-3c represent high and very high magnification SEM micrographs of the deposited films respectively. As can be seen in Figure 4-3b, good particle integrity is obtained and particles are flocked together into agglomerates penetrating into each other.

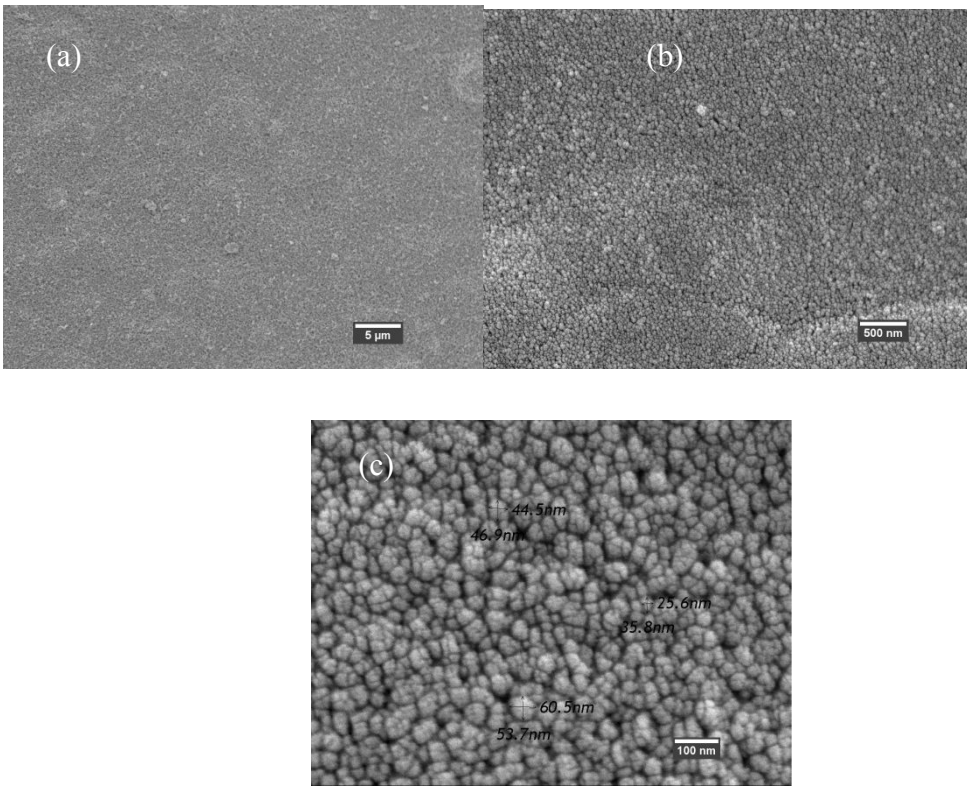

Figure 4-3.a: Low magnification SEM surface view of the deposited films. **b:** High magnification SEM micrograph of the deposited films showing uniform surface characteristics. **c:** Very high magnification SEM micrograph showing grain size of the deposited films.

The main advantage of ESD lies in the fact that the deposition process is very simple and is carried out at room temperature. Realization of the presented results at room conditions and open environment is an achievement and it is believed that with more improvements in the nanoparticles alcosol ink, ESD can be the most sought after deposition process for manufacture of thin films. Grain size can be obtained from Figure 4-3c, and as is witnessed in the micrograph, it ranged between 20 nm to 30 nm and hence it can be assumed that the average grain size was somewhat around 25±5 nm.

4.2.2 Thickness Analysis

Thickness was measured at 10 different points on the film and thus the average thickness of the film came out to be approximately 115±20 nm which is exceptional as far as the requirements for the different electronic devices are concerned.

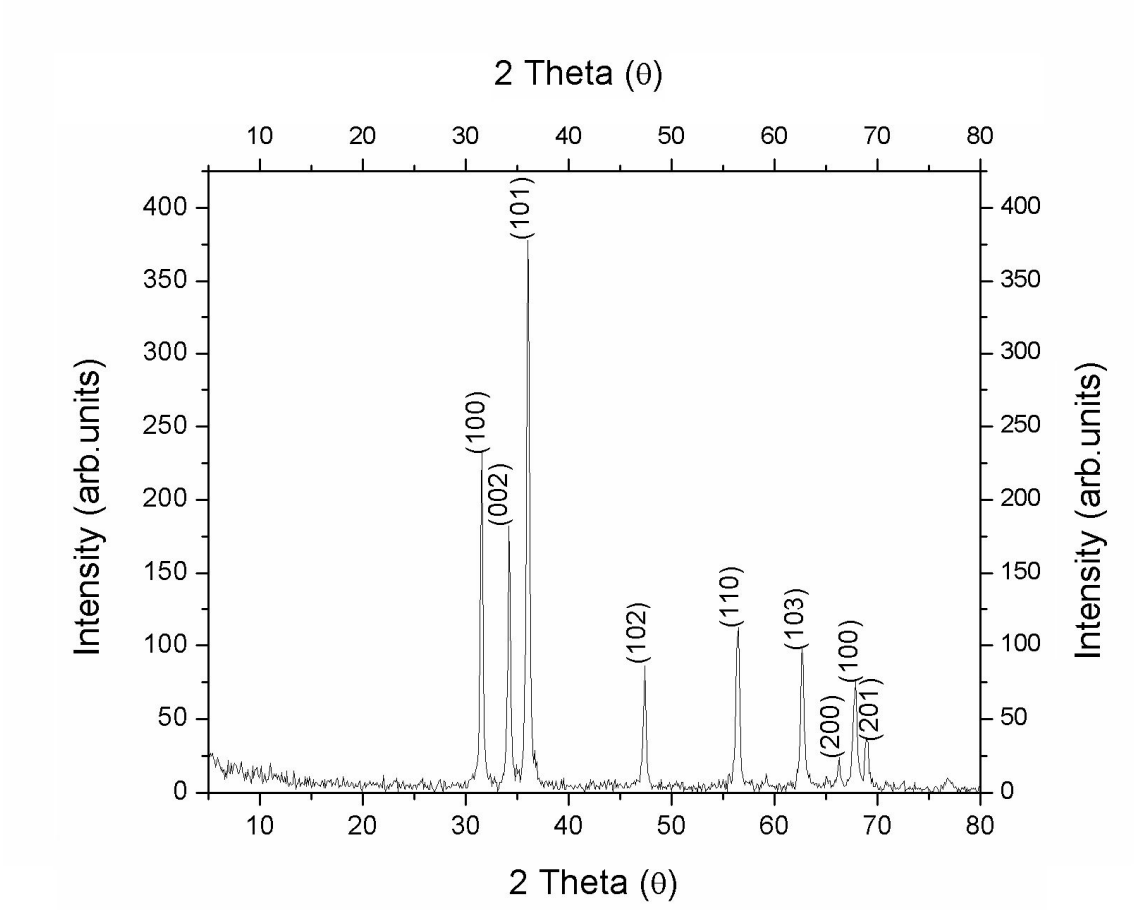

Figure 4-4.XRD analysis representation of the deposited layer. Observed peaks confirm the wurtzite crystal structure.

4.2.3 Phase Characterization

The XRD analysis of ZnO nanoparticles sample yielded a plot of intensity versus angle of diffraction as shown in Figure 4-4. The ZnO nanoparticles diffraction peaks agree with JCPDS card No: 36-1451, which corresponds to the hexagonal wurtzite structure with space group $C_{6v}(P6_3mc)$. The average particle size of crystal is 26 nm. It was determined by Scherrer's equation:

$$D = \frac{k\lambda}{\beta \cos\theta} \qquad (4\text{-}3)$$

Where D is crystalline size, λ is the radiation wavelength (1.5406 Á), β is the peak full width at half maximum, θ is the diffraction angle and k = 0.94 for spherical shape particles.

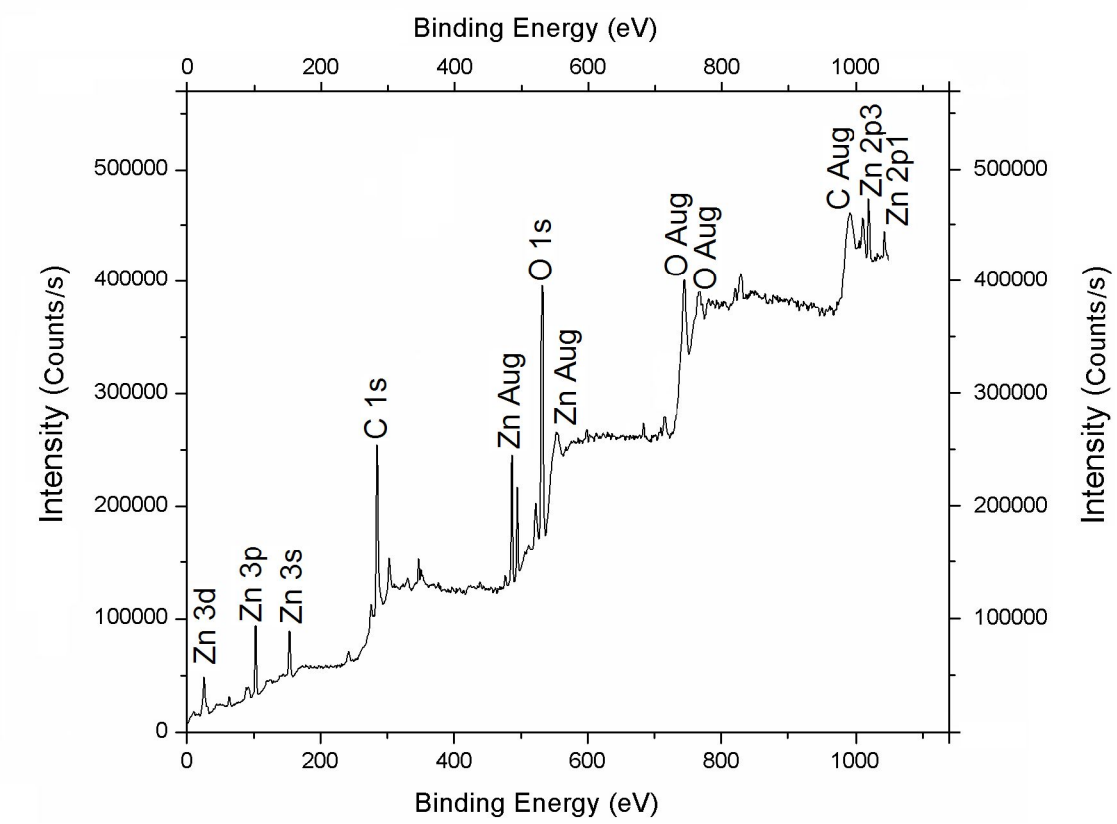

Figure 4-5.XPS analysis representation of the deposited layer. Peaks of Zn, O and C are marked accordingly.

4.2.4 Purity Analysis

Figure 4-5 represents the marked XPS graph for ZnO films deposited on bare glass. All of the peaks on the curve are ascribed to Zn, O and C elements and no identifiable peaks of other elements were observed. The presence of carbon comes mainly from the residuals from the alcohol [Habibi&Sheibani 2010]. Therefore, it is

concluded that the sample is composed of Zn and O, which is in good agreement with the XRD analysis.

4.2.5 Electrical Characterization

ZnO films made without any intentional doping exhibit n-type conductivity, caused by a deviation from stoichiometry due to native defects. Traditionally, two intrinsic defects are reported in the literature as dominant background donors in ZnO, namely the oxygen vacancy (V_O) and interstitial Zn (Zn_I) [Song 2008].

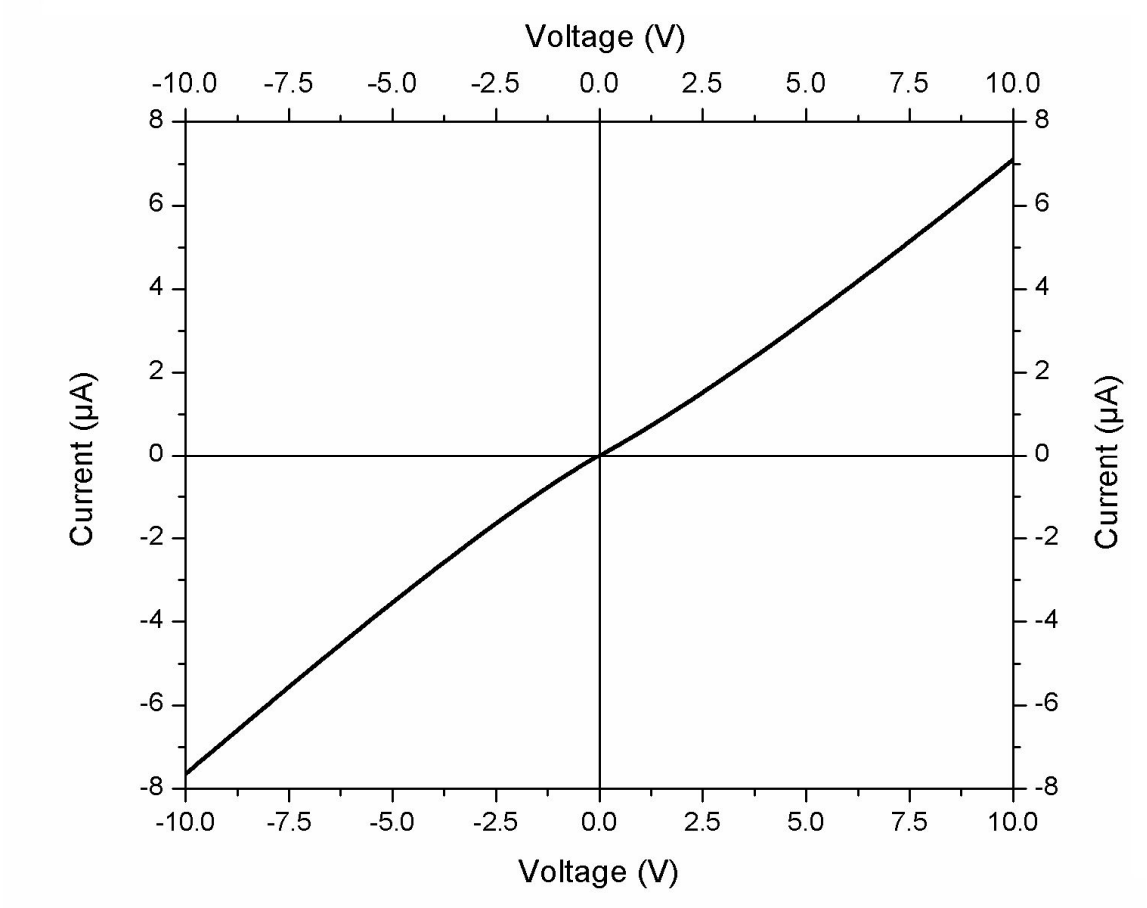

Figure 4-6.I-V characteristic curve of the deposited ZnO films.

The I-V characteristic curve of the deposited films is given in Figure 4-6. The graph shows a good ohmic behavior with a negligible non-linearity at low voltages. This behavior can be attributed to minor charge trapping in the film [27]. The resistivity

was calculated from the slopes of the linear I-V plot and using the sheet resistivity formula for a thin film:

$$\rho = \frac{\pi t}{\ln 2}\left(\frac{V}{I}\right) \qquad (4\text{-}4)$$

wheret is the film thickness (115 nm), while V and I are voltage and current from the I-V plot. The resistivity was found out to be ~64 Ω.cm.

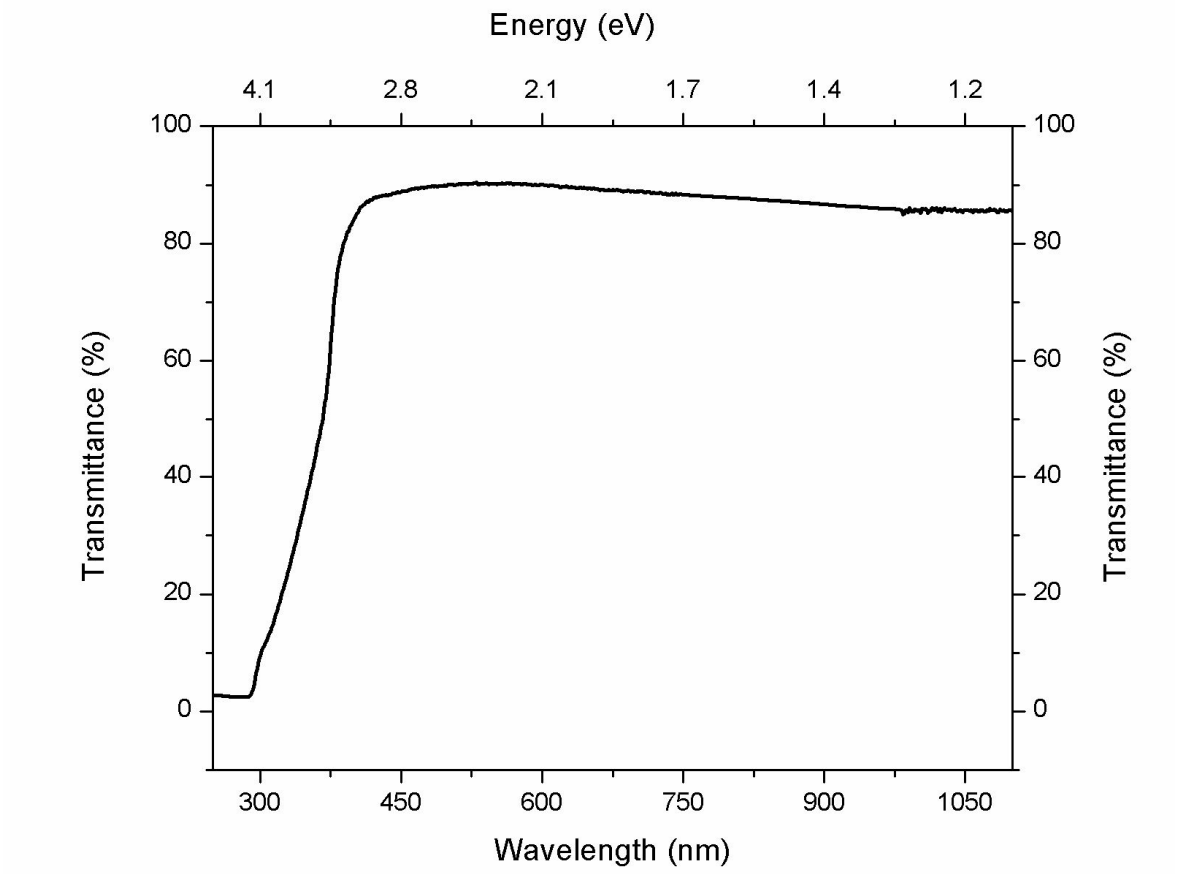

Figure 4-7. Transmittance spectra of the deposited films with respect to wavelength (nm) and energy (eV) of incident light in UV, visible and near-infra-red spectrum confirms good transparency of the films.

4.2.6 Optical Characterization

Figure 8 shows the transmittance spectra of the ESD deposited films for ZnO against the wavelength of the incident light and energy in ultra-violet (UV), visible and near-infra-red (NIR) spectrum. The layers exhibit good performance in visible and NIR spectrum where the average transmittance is around 88%. Based on the data, the energy band gap (E_g) has been calculated and comes out to be 3.3 eV.

5. Deposition of Aluminium doped Zinc Oxide films

ESD has become an alluring research area for researchers around the world because of its immense applications in industry and research. Direct deposition of nano-particles' solution of functional materials for their use in micro-electronic devices is one of the major applications of ESD. As discussed earlier, ESD involves the flow of a solution or dispersion, under the stimulus of an electric field at ambient conditions. The applied electric field deforms the liquid into a cone at the exit of a thin micron-scale metallic capillary and from the cone apex a jet evolves. The droplets generated from the spray are deposited on a substrate to form a uniform film of the solute present in the working liquid. Main advantages of ESD include the simple process with no high temperature requirements and low costs involved.

Transparent conductive oxides, find extensive applications in optoelectronic devices like solar cells, liquid crystal displays and heating mirrors where conductivity and transparency both play an important role in increasing the efficiency of the corresponding device. ZnO:Al therefore has attracted immense attention lately because of its large band-gap, higher conductivity, chemical and thermal stability and abundance. Aluminum doped zinc oxide (ZnO:Al) is also commonly used as transparent window layer in thin film solar cells. In combination with $Cu(In,Ga)Se_2$ (CIGS) absorber layers, solar cells with efficiencies of up to 18.8 % have been obtained [Contreras et al. 1999]. Several deposition techniques are already in the market to grow (ZnO:Al) thin films which include chemical vapor deposition [Yee et al. 1996] magnetron sputtering [Ellmer et al. 1997], spray pyrolysis [Seeber et al. 1999] pulsed laser deposition [Sakai et al. 2008], sol-gel method [Musat et al. 2004], atomic layer deposition [Kumar et al. 2010] and molecular beam epitaxy [Minami et al. 2003].

In this paper, ESD has been utilized to deposit highly transparent, 250 nm thick films of ZnO:Al on glass substrates at ambient conditions. The stimulus for this work has been taken from our recent study in which i-ZnO layers have been fabricated using

ESD process [Muhammad et al. 2012]. Nano-colloid solution of ZnO:Al has been made by dispersing commercially available aluminum doped zinc-oxide nano-particles in ethanol. Although many modes of atomization exist in ESD namely micro-dripping, spindle, cone-jet and multi-jet, cone-jet mode of atomization has been deployed here to achieve the uniform films as near-monodispersed droplets of few micrometers in size are generated by this mode [Choi et al. 2012, 11]. No other instance has been reported where such deposition technique for ZnO:Al deposition has been used, therefore the present study is a useful addition in the deposition schemes of ZnO:Al. In addition the present study is a rare instance of direct deposition for the ZnO:Al films at ambient conditions without involving expensive plasma and vacuum generation equipments. This chapter discusses a comprehensive description of ZnO:Al film formation and characterization from the nano-particles alcohol suspension preparation to film deposition through ESD and its complete characterization. The layers surface morphology is characterized through the scanning electron microscope (SEM) and atomic force microscope analysis and thickness measurements are performed deploying a non-invasive commercially available thickness measurement system. Crystal structure is confirmed through x-ray diffraction (XRD) and the electrical properties (IV curve) of the film are tested to verify the fitness of deposited films to be used in electronic devices. Surface composition analysis has been carried out by x-ray photoelectron spectroscopy. The presence of Aluminum has been further analyzed using Fourier Transform Infra Red (FTIR) spectroscopy. Moreover optical characterization of the films is obtained by a UV/VIS/NIR spectrophotometer.

5.1. ZnO:AlNano-particles' Solution Preparation

6 % Aluminum doped zinc-oxide nano-particles (ZnO/Al_2O_3 – MKBF7871) were obtained from Sigma-Aldrich and were used as received. Non-ionic surfactant, Triton X-100 (Sigma-Aldrich) was used as a wetting agent. The solid content was kept at 10 wt.%. The nano-particles dispersed in 99.9 % pure ethanol (OCI Company Ltd.) and 0.05% Triton X-100, were sonicated for 10 minutes, 3:1 as on-off ratio, at 20 Watts. The solution was then stirred for 72 hours at 70 ^{o}C using a magnetic stirrer at 1500 RPM. The physical properties of the solution were measured by conductivity

meter (EUTECH Instruments - ECOSCAN CON 6) and surface tension meter (SEO-Phoenix). The conductivity and surface tension of the ink were measured to be 115.5 μS/cm and 0.0355 N/m respectively. The density of the solution was recorded as 1125 Kg/m^3. The measurement of viscosity was carried out with a stain-controlled viscometer (SekonicViscomate VM-10A) and viscosity was recorded as 7.8 cps. Dielectric constant of the liquid affects the ESD process tremendously and hence it is a very important parameter to verify the occurrence of classical ESD. The dielectric constant of the solution was measured using a dielectric constant meter (BROOKHAVEN INSTRUMENTS CORPORATION 870 Liquid Dielectric Constant meter) and was calculated as 33.

5.2. Experiment Details

The films were deposited on glass substrates (Corning 7059) through ESD at room conditions at a substrate speed of 0.30 mm/sec and at a distance of 10 mm between the capillary and the substrate. Before the deposition process, the substrate was rinsed with acetone and then irradiated with UV light in the UV cleaner for 15 minutes. The deposited films were sintered at 500 ^oC for 6 hours before the characterization process. A scanning electron microscope (SEM), Jeol JSM-7600F, was used to characterize the surface quality of the deposited films at 5 kV. An atomic force microscope (AFM), P-AFM100, has been used to confirm the layer uniformity in contact mode. Cantilever-type probe is used with trapezoidal cross-section. The back-side width of the cantilever is approximately 40 μm. Film thickness was measured by a non-destructive thin film thickness measurement system K-MAC ST4000-DLX based on the principle of constructive and destructive interference in the spectrum of white light incident on the surface of the film. The crystal structure of the films was verified by x-ray diffraction (XRD) measurements carried out by using Rigaku D/MAX 2200H, Bede Model 200 system. Cu-Kα radiation (λ = 1.054 nm), from the X-ray generator operating at 40 kV at 30 mA was used to record the X-ray diffraction patterns. A scan resolution of 0.25^o was used for the measurements and diffraction intensity was recorded in the 2θ range 0 – 85^o. The X-ray photoelectron spectroscopy (XPS) analysis of the deposited thin film has been carried out using VG Microtech XPS analysis equipment using Mg-Kα radiation

from an X-ray source operating at 12 kV, 15 mA. The survey spectrum was taken at pass energy of 50 eV, providing an instrumental resolution of 1 eV. The scan was done between 0 eV to 1080 eV. The current-voltage (IV) characteristic curve of the deposited films was measured by Agilent B1500A Semiconductor Device Analyzer. Measurements were carried out with a hold time of 2 seconds and the scan resolution of 30 mV. The transmittance spectrum of the deposited films has been obtained by using the Shimadzu UV-3150 UV/VIS/NIR spectrophotometer in the range of 250 nm to 750 nm covering the ultraviolet and visible regions.

The films were investigated by a FTIR analyzer (Bruker IFS 66/S, Germany) for analysis of functional groups present in the film. ZnSe beam splitter was used and the machine was operated at a resolution of 1 cm^{-1} within the spectral range of 400–2000 cm^{-1} at room temperature with power rating of 30 Watts.

5.3. Results and Discussion

5.3.1 Cone-jet and Spray Formation

As discussed earlier different spraying modes occur during the ESD process. The occurrence of these modes depends upon the applied voltage, flow rate and the physical properties of the liquid, namely density, viscosity, surface tension, relative permittivity and electrical conductivity. A complete account on ESD modes can be found in chapter 2 of this thesis. The ZnO:Al nano-particles' solution remained completely stable during the experiments with no sedimentation which could have caused nozzle blockage. The main controlling parameter in ESD is the flow rate of the solution as it directly dictates the meniscus generation at the nozzle exit. Hence it is very important to use the appropriate flow rate of the solution. A usual approach is to make an operating envelope of the solution, i.e. the detection of a range in which the solution will exhibit the cone-jet mode. Therefore starting from 25 µl/hr, the ESD behavior was noted for each flow-rate with a step of 50 µl/hr until the phenomenon of stable cone-jet vanished. At each flow rate step, applying different magnitude of voltage gives a different mode of atomization and hence various modes were observed such as dripping, micro-dripping, pulsating cone-jet, stable cone-jet and multi-jet. Figure 5-1 provides the observed operating envelope of the ZnO:Alsolution

representing different atomization modes with varying flow rates and corresponding applied voltages. The stand-off distance i.e. the distance between the nozzle exit and substrate was kept at 1 cm.

A major effect of different flow rates can be found on the achieved layer thickness. A complete analysis was carried out to get the knowledge of optimized flow rate to achieve the desired thickness and the effect of flow rates on the layer thickness. Film thickness was measured at 10 different points on the film for each flow rate.

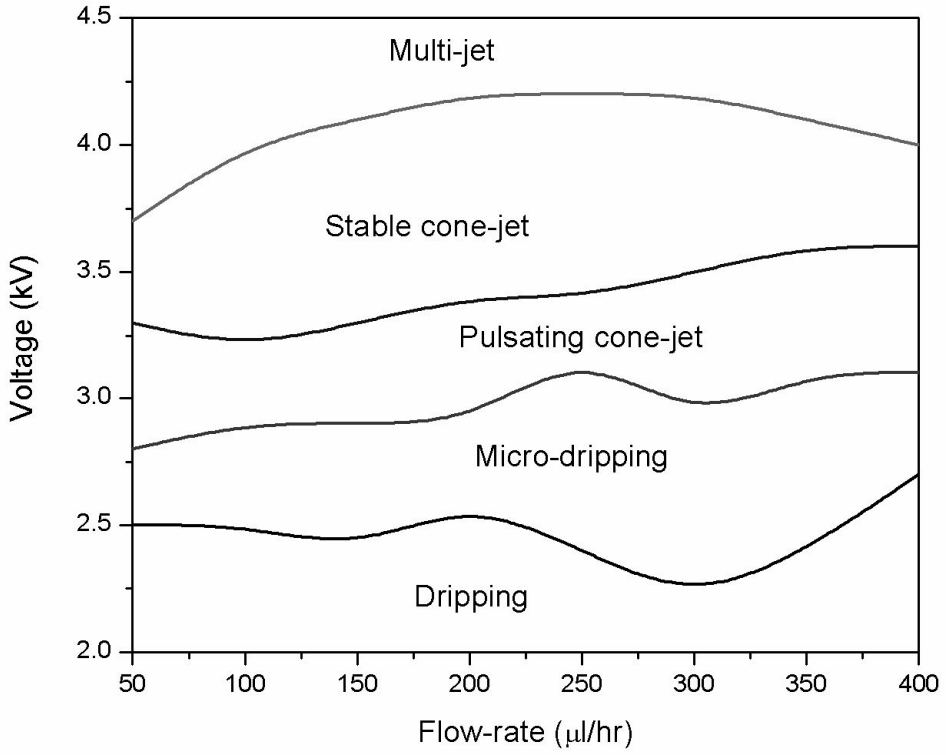

Figure 5-1. Operating envelope representation for different electrospray regimes according to flow rate and applied voltage.

Figure 5-2gives the representation of variation in film thickness w.r.t changing flow rates. Average thickness achieved for 50, 100, 150, 200, 300 and 400 μl/hr was ~ 72, 145, 240, 335, 495 and 633 nm respectively within the confidence level of 95% of the sample size of 10 points. 150 μl/hr was selected as the flow rate for final film

fabrication. Figure 5-3 represents high zoom and high speed images of different atomization modes as achieved at 150 μl/hr flow rate when different voltages were applied. Stand-off distance has been kept at 1 cm. At zero voltage, dripping mode was observed. When the voltage was increased from zero up to 2.5 kV, micro-dripping mode was observed. From 2.8 kV, pulsating cone-jetting mode appeared which went until 3.3 kV and after that until 4.1 kV the stable cone-jet regime was observed. After 4.1 kV multi-jet mode occurred. With further increase in voltage, the jet discharged.

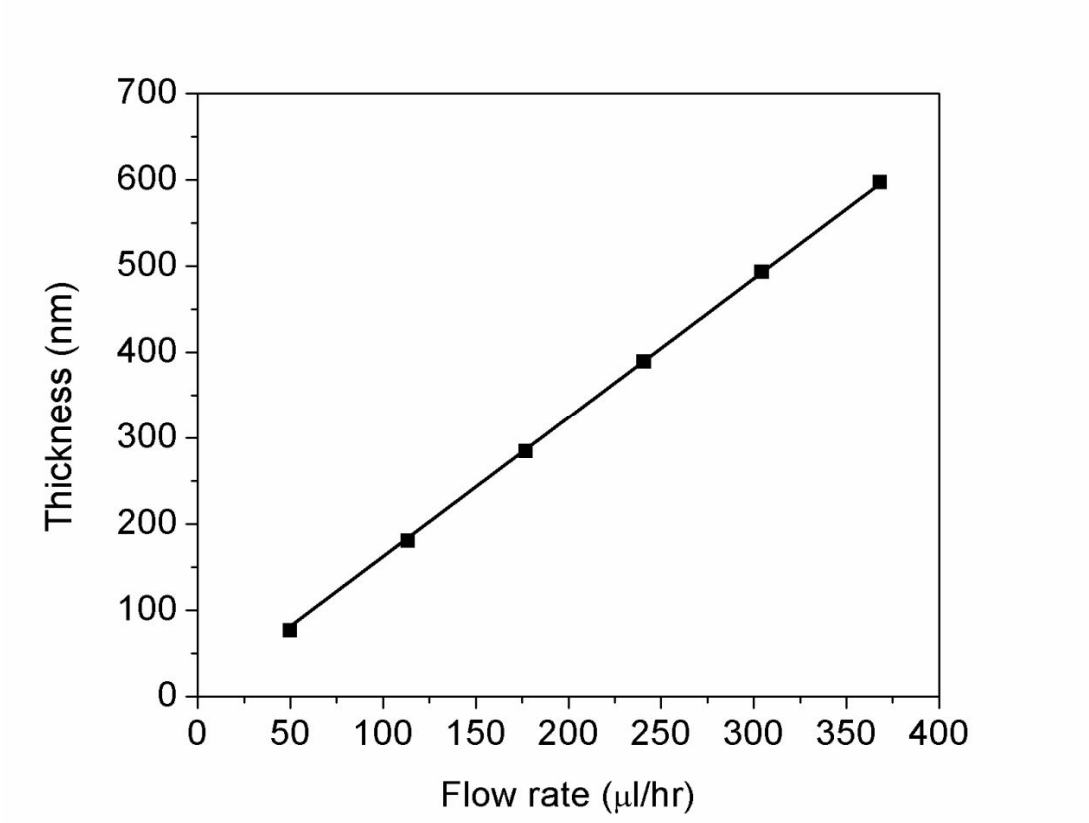

Figure 5-2. Variation in thickness w.r.t. applied flow rate.

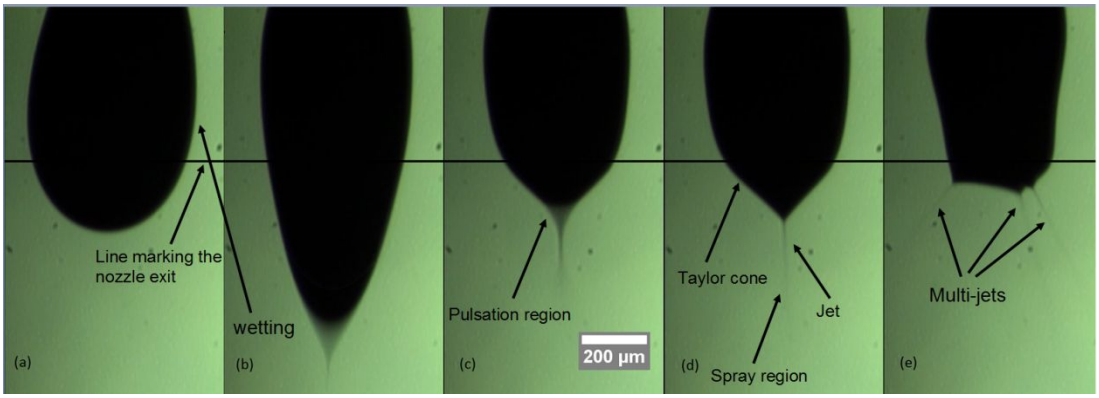

Figure 5-3. Different electrohydrodynamic atomization modes observed during the deposition process. **a:** dripping **b:** micro-dripping, **c**: pulsating cone-jet mode, **d:** stable cone-jet mode and **e:** multi-jet.

As mentioned earlier, it is important to verify the occurrence of classical hydrodynamic atomization for the process to be repeatable and consistent with the theory. The occurrence of the classical electrohydrodynamic atomization requires the hydrodynamic time $T_h$to exceed the charge relaxation time T_q. The two quantities are given as [Ganan-Calvo et al. 1994,Samarasinghe et al. 2008]:

$$T_h = \frac{LD^2}{Q} \tag{5-1}$$

$$T_q = \frac{\varepsilon_0 \varepsilon_r}{K} \tag{5-2}$$

Where, L denotes the axial length of the jet, D is the jet diameter, Q is the flow rate and K is the electrical conductivity. According to Figure 5-3, using the following values for these quantities,

$L = 190\,\mu m$
$D = 18\,\mu m$
$Q = 150\,\mu l/hr = 6.111\times10^{-11}\,m^3 s^{-1}$
$\varepsilon_r = 33$
$\varepsilon_0 = 8.85?\ 0^{-12}\ \mathrm{Fm}^{-1}$
$K = 0.01155\ S\mathrm{m}^{-1}$

Implies that $T_h = 0.001$ seconds which is much greater than $T_e = 2.53 \times 10^{-8}$ seconds. Thus, the required condition for classical electrohydrodynamic atomization is satisfied [Ganan-Calvo et al. 1994].

5.3.2 Surface Characterization

Figure 5-4 shows the SEM micrograph of the deposited film at moderate magnification. As can be seen, particle integrity is appreciable and particles are flocked together into uniform agglomerates penetrating into each other. The layer gives a uniform impression and decent results are achieved keeping in view the room conditions' deposition. Some pores are visible however, which become more apparent at very high magnified image (inset) but since the magnitude of these pores is of the order of certain nano-meters, it can be concluded that presentable layer quality has been achieved and the films can be used in micro-electronic applications without any problem. The high magnification image of the deposited layer gives a hint of non-uniformity as well.

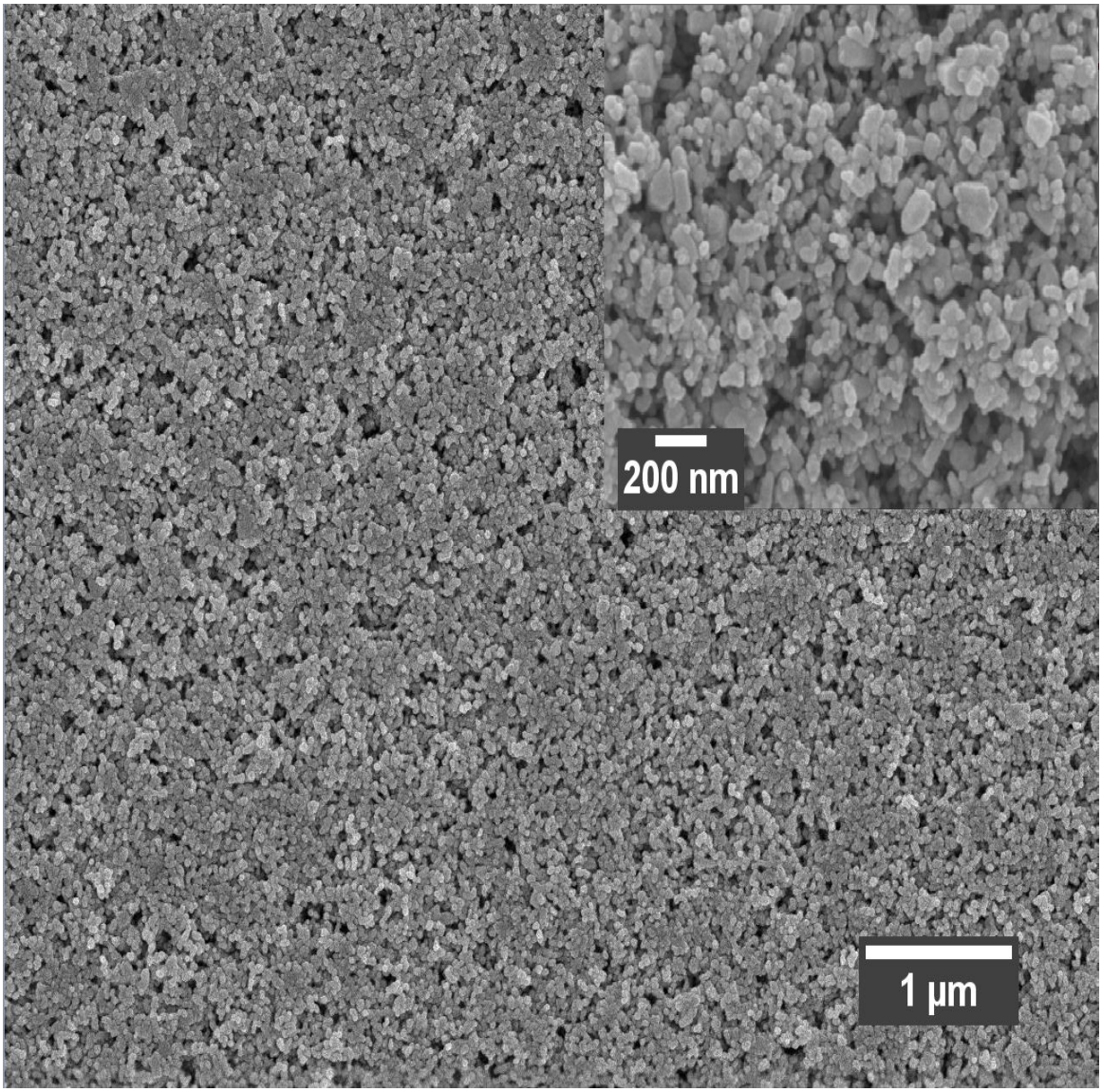

Figure 5-4.SEM surface view of deposited films showing a fine surface morphology at lower magnification. The inset shows non-uniformity at high magnification.

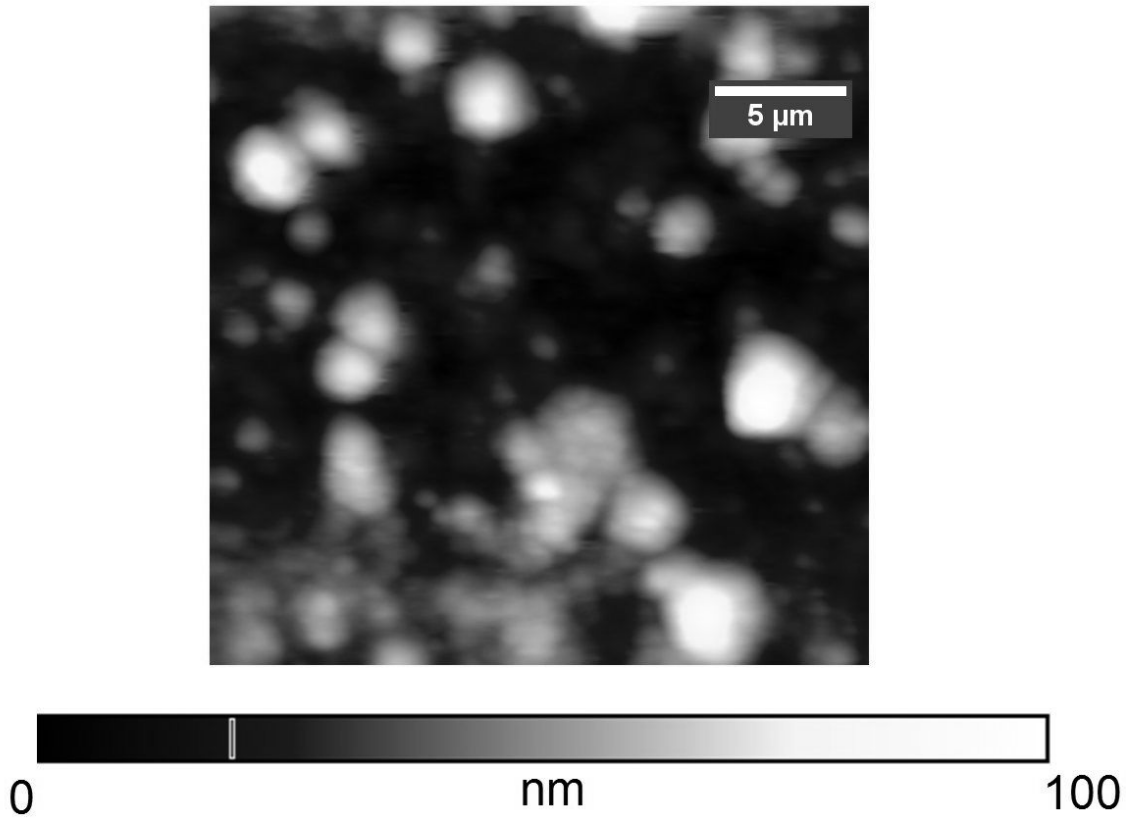

Figure 5-5.AFM image of the layer. The formation of hillocks is obvious from the image.

Figure 5-5 represents the 2D AFM micrograph of a 25 µm × 25 µm patch of the layer. The deposited layer has a morphology which contains several hillocks which are attributed to the induced charges on the substrate surface present because of the strong electric field between the nozzle and ground. A detailed note on this behavior has been given in [Chen et al. 1996,Muhammad et al. 2012]. Apart from these spikes, the layer roughness is satisfactory but not excellent and it leaves an area of further research to overcome this drawback. Since the main application of transparent conductive oxides like ZnO:Al is usually top electrode, hence the drawbacks of porosity and non-uniformity, of the level found in the present study literally does not matter much and the films are fairly usable in those intended applications. Accomplishment of the presented results at room conditions and open environment is an achievement and it is believed that with more improvements in the nano-particles solutions and process, ESD can be the most preferred deposition process for manufacture of window layers in particular and thin films in general.

5.3.3 Transmittance Characterization

Figure 5-6 shows the transmittance spectra of the ESD deposited ZnO:Al films against wavelength of the incident light in ultra-violet (UV) and visible spectrum.The layers exhibit excellent transmittance and the average transmittance in the visible region is around ~93%. Based on the data, the energy band gap (E_g) has been calculated and comes out to be ~3.5 eV.

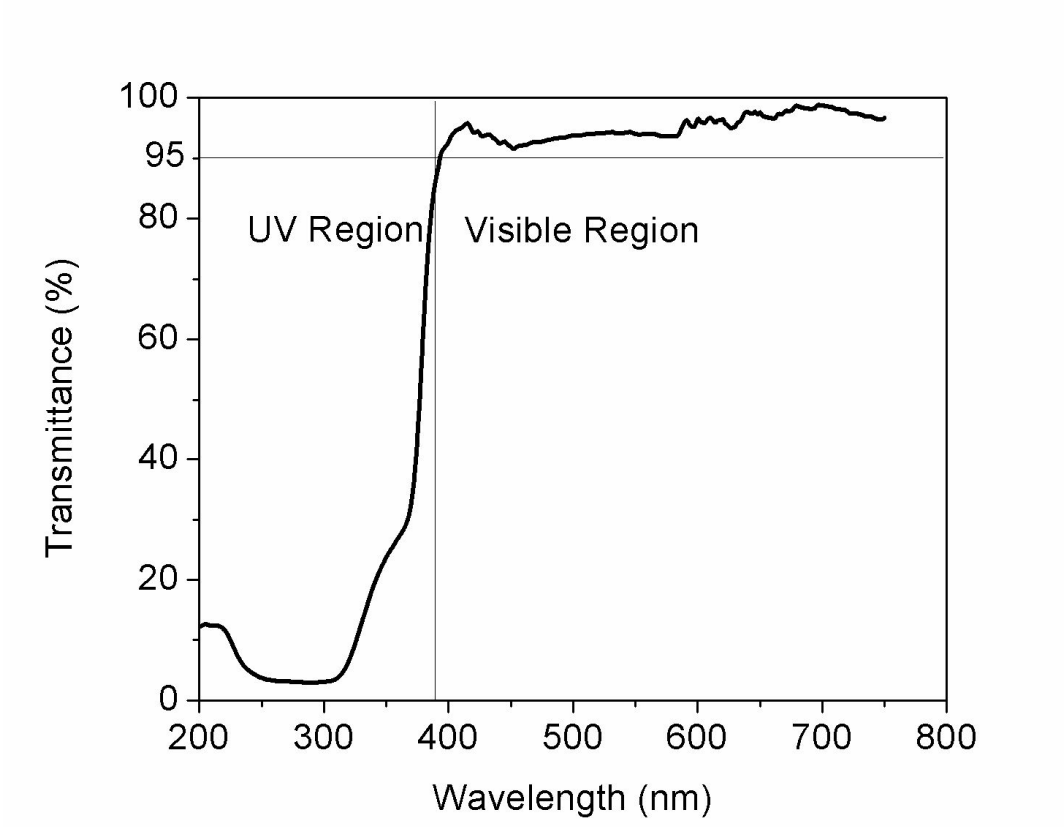

Figure 5-6. Transmittance spectra of the deposited films with respect to wavelength confirms excellent transparency of the films up to 93% on average in the visibleregion.

5.3.4 Electrical Characterization

It is commonly known that sintering temperature plays an important role in the sheet resistivity of thin films. Therefore to get a complete picture, deposited films were sintered at different temperatures but for the same time, i.e. 6 hours. IV characteristic curve of the deposited films, is given in Figure 5-7. The resistivity was calculated

from the slopes of the linear I-V plot and using the sheet resistivity formula [Muhammad et al. 2012] for a thin film:

$$\rho = \frac{\pi t}{\ln 2}\left(\frac{V}{I}\right) \qquad (5\text{-}3)$$

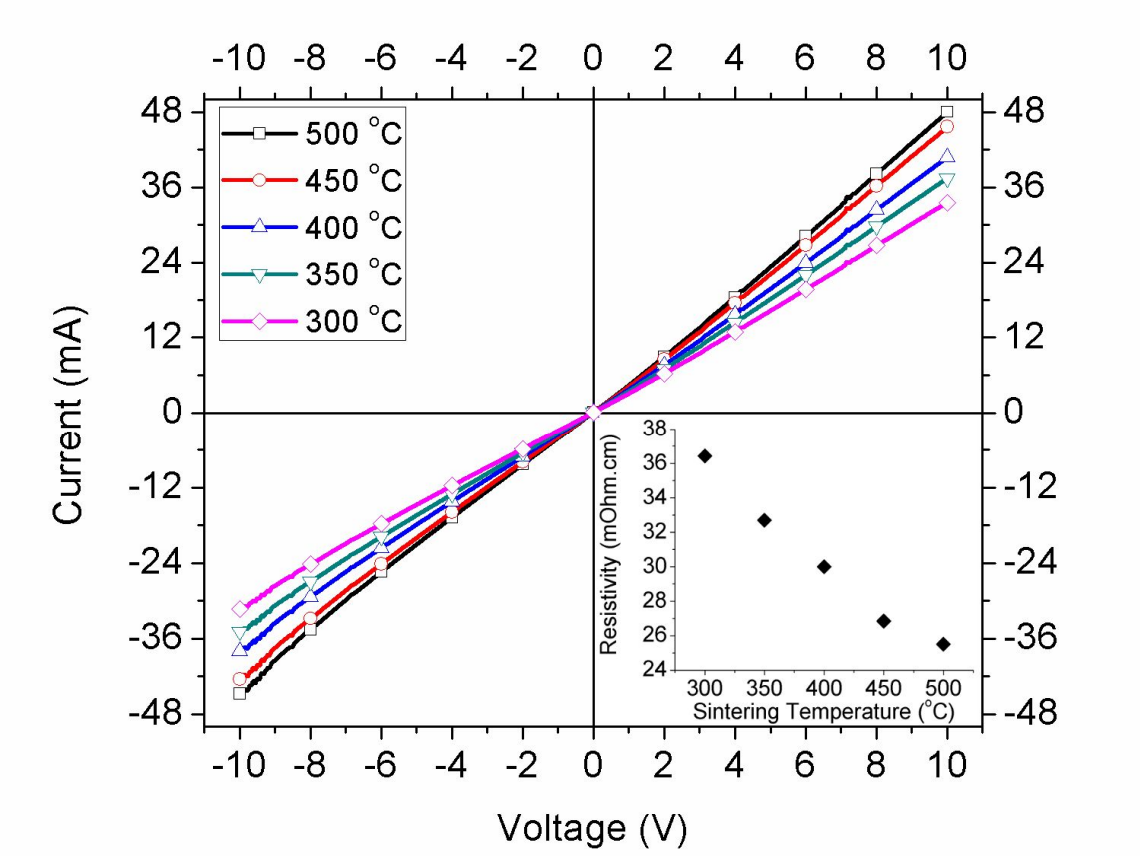

Figure 5-7.I-V characteristic curves of the deposited films at different sintering temperatures. Inset shows the variation of resistivity w.r.t. sintering temperature.

wheret is the film thickness (250 nm), while V and I are voltage and current from the I-V plot.. As can be seen, the resistivity decreases with increase in sintering temperature and minimum resistivity was found at sintering temperature of 500^{o}C while the maximum resistivity was found at 300^{o}C sintering temperature. The inset in Figure 5-7 shows the resistivity variation with respect to sintering temperatures. The minimum resistivity calculated was ~25 mΩ.cm at 500^{o}C sintering temperature.

5.3.5 Structural Characterization

The deposited layers, sintered at 500 ^{o}C were analyzed for purity and structure characterization using the x-ray diffractometer system. XRD patterns, as presented in Figure 8, revealed the existence of both zincite (JCPDS 36-1451) and gahnite (JCPDS 5-0669) phases. Gahnite phase ($ZnAl_2O_4$) was segregated along the ZnO grain boundaries.

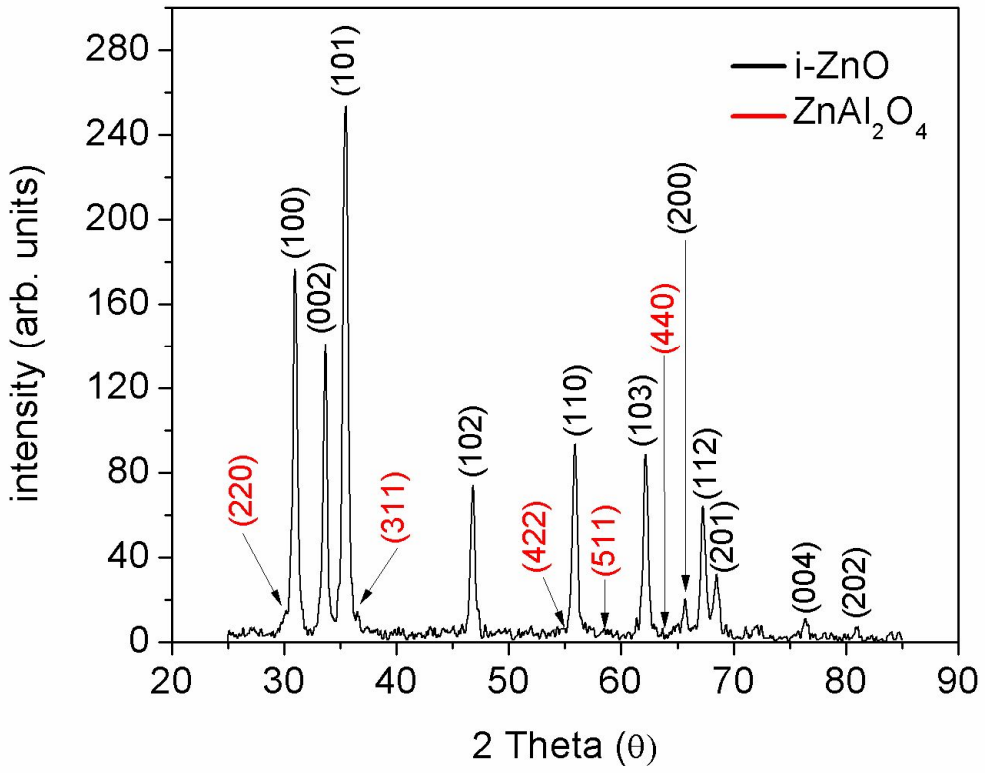

Figure 5-8.XRD analysis of the deposited films showing the presence of zincite (black) and gahnite (red) phases.

5.3.6 Purity Analysis

Figure 5-9 shows the XPS analysis for the deposited films on highly doped conducting silicon substrates. The Al 2p peak is prominently identified at

approximately 73 eV while Zn 2p1 and Zn 2p3 peaks are identified at 1023 and 1048 eV respectively and O 1s peak is identified at 543 eV. Therefore the XPS analysis confirms that the deposited films are of high purity and composed of Zn,Al and O, which is in good agreement with the XRD analysis. Si peak is there because of the substrate and a little carbon is also there that might arise from the residuals from the alcohol.

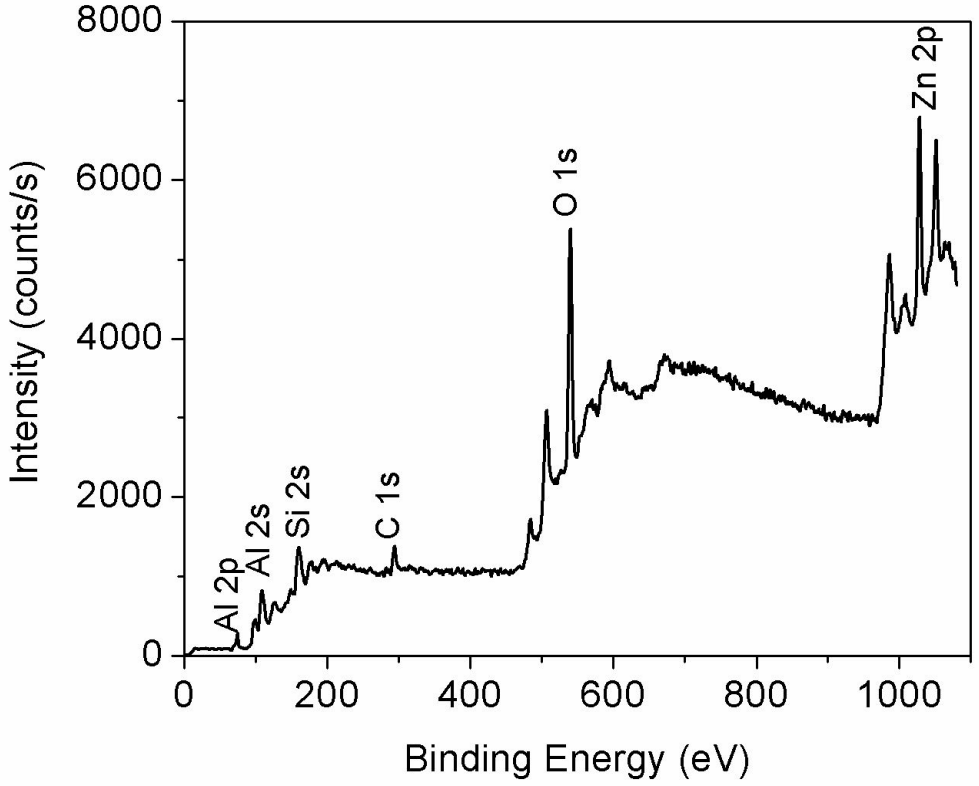

Figure 5-9.XPS graph of the deposited ZnO:Al layers on Si substrates. Al and Zn, O, Si and C peaks are marked accordingly.

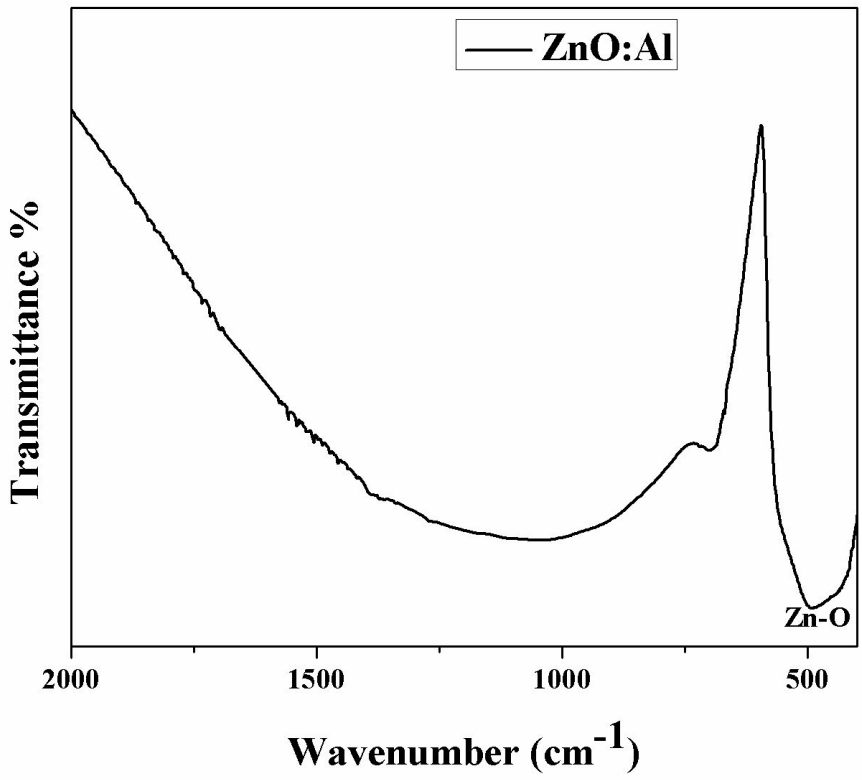

Figure 5-10.FTIR spectra showing shifted peak for Zn-O confirming the presence of Al in the films.

The deposited films were also investigated by FTIR spectroscopy analysis for further confirmation of the presence of aluminum in the samples and purity of the films. Figure 10 shows a more intense peak at 480 cm^{-1} that can be assigned as Zn-O stretching frequency due to presence of dopant atoms of aluminum [Yogalmar& Bose 2011]. When aluminum is introduced as a doping material, the mode of vibration of Zn-O peak shifts basically from lower wavelength region to the higher wavelength region which is the reason this peak is at a higher wavelength than that of pure ZnO which usually occurs at around 440 cm^{-1}. The plot also shows one shoulder peak corresponding to Al-O in the range of 680 - 670 cm^{-1} [Wan et al. 2008]. There are no any other characteristic peaks, which indicate the purity of deposited thin films.

6. Executive Summary

This thesis is a comprehensive study of the fabrication of thin films of functionalmaterials using a novel method known as Electrospray Deposition (ESD). This is the first account where ESD is being utilized for different functional materials' deposition and the films are characterized thoroughly taking ESD in competition to the existing thin film deposition techniques like chemical vapour deposition,lithography, plasma related techniques and physical vapour deposition techniques. Although many scientists and researchers have adopted ESD their research topic, yet usually ESD has been utilized in mass spectroscopy and powder production applications. A lot of research has been carried out where ESD is used for printing metallic patterns and some research groups claim commercial applications as well, however deposition of fully characterized working functional thin films via ESD has been at its very early stages. Therefore this thesis has been carried to elucidate ESD as a proven method for functional thin films deposition and ultimately a method for successful thin film device fabrication. The thesis involves the fabrication of three different types of thin films where one is a chalcopyrite compound of Copper, Indium and Selenide i.e. CuInSe2 (CIS). Second is an intrinsic metal oxide compound of Zinc and oxygen i.e ZnO and last is a doped metal oxide i.e. Aluminium doped ZnO (ZnO:Al). CIS is used as absorber layer in the second generation solar cells while ZnO and doped ZnO:Al are very useful materials in many micro-electronic and opto-electronic devices as semiconducting and transparent conductive oxide layers respectively. The thesis first discusses the conventional methods of thin film deposition, their benefits and drawbacks and then motivation of this thesis is emphasized by highlighting how ESD caters for the drawbacks of the conventional methods by its cost effectiveness and room temperature deposition process. In the second chapter theoretical basics of ESD are discussed briefly including working principle and important atomization modes that is dripping, micro-dripping, unstable and stable cone jet mode and multi-jet mode. Then effect of different material physical properties of the inks i.e. conductivity, viscosity, surface tension etc are elaborated. Effect of process parameters like electric field strength, flow rate and nozzle diameter are discussed as well. Third chapter discusses nano-particle solution processing route to the cost effective and easy

fabrication of CIS layers via electrospray deposition of six different inks containing CIS nano-particle colloid solutions. CIS nano-particles are first synthesized using solvo-thermal process and then six types of inks have been prepared which differ on the basis of solvents and particle concentrations. The chapter discusses the deposition of ~1 μm thick CIS layers on Molybdenum coated glass substrates. The assessment of deposited layers on the basis of their jetting behavior, surface integrity, structural analysis, surface composition and transmittance behavior through ESD, scanning electron microscope, XRD analysis, XPS analysis and optical analysis along with electrical characterization of the films has been discussed in detail.

Next chapter elaborates deposition of thin films of ZnO where an alcosol solution containing 7 wt.% ZnO nano-particles was synthesized first and an average thickness of 115 nm at a constant substrate speed of 0.1 mm/s is achieved via ESD. Pure and perfectly uniform transparent films with an average transmittance of 88% have been deposited with wurtzite crystal structure and an electrical resistivity of approximately 64 mΩ.cm.

Lastly the deposition of ZnO:Al films has been discussed where a 10 wt.%monodispersed solution containing 6% ZnO:Al nanoparticles (ZnO/Al2O3) in ethanol was synthesized first and then used in the deposition process as the working solution. Pure and uniform transparent films with an average transmittance of 93% have been deposited with crystal structure exhibiting both zincite and gahnite phases. Surface composition purity was confirmed using x-ray photoelectron spectroscopy technique and the clear indication of Zn-2p and Al-2p peaks confirm surface integrity. Fourier Transform Infrared analysis is further provided which confirms the presence of aluminum in the samples. The current-voltage (IV) characteristics and the resistivity were estimated from the slope of the IV-curve which was approximately 25 mΩ.cm. The layer roughness characterization is discussed as well which was carried out using atomic force microscopy. The unique advantage which ESD technique carries is that of being a much cheaper and easy solution for the manufacture of thin film devices at standard room conditions and this thesis hence illuminates ESD as an alternative to conventional techniques.

7. Conclusions and Future Work

Electrospray deposition of the CIS absorber layers has been discussed using nanoparticle based CIS inks. The unique advantage which ESD technique carries is that of being a much cheaper and easy solution for the manufacture of photovoltaics at the standard room conditions. Six different CIS nano-particles based inks have been synthesized with different surfactant compositions and particle concentrations. Layers with good morphology have been obtained with inks with higher particle concentration and higher Terpineol concentration in the solvent. However excessive amount of Terpineol and particle concentration resulted in thicker films, therefore it is concluded that 1:1 (Ethanol:Terpineol) solvent composition and 12.5 wt% particle concentration is the most suitable ink composition. Films show chalcopyrite structure and the existence of interfacial MoSe2 layer has been confirmed via XRD analysis. The XPS analysis shows that films are pure however trace amounts of carbon are there, whereby carbon concentration increases as the percentage of Terpineol increases in the solvent. Films exhibit good optical properties where films with less particle concentration suffer from relatively higher optical transmittance. Films with higher particle concentration inks show excellent average transmittance of just 10% in the visible region. Films show good linear I-V relationship in the low voltage region while a good overall semiconductor behavior is shown in all the films. However electrical performances suffer with the layers with inks containing less particle concentration and higher amount of Terpineol in the solvent. Keeping in view ink stability, operating parameters of electrospraying and film characterization results, it is therefore concluded that CIS-5 is best suited for its use in electrospray processing of CIS films for solar cell fabrication process.

The 7 wt% alcosol solution containing ZnO nanoparticles fully dispersed in ethanol was used to produce high quality ZnO films on glass substrates via electrospray deposition. Moderate voltage requirements, room temperature deposition and simple process are remarkable characteristics of this atomization technique. The deposited layers have a wurtzite crystal structure with good surface morphology and ~115 nm

film thickness. Film composition has been confirmed by XPS analysis as well. The transmittance spectrum of the achieved films shows good transparency of films with around 88% transmittance. IV characteristics of the deposited films show good linear Ohmic behavior with a sheet resistance of 64 mΩ.cm. The characterizations process confirms the quality of the deposited films through ESD to be viable for their use inphotovoltaics, thin films transistors and many other micro-electronic devices.

A simple solution for the deposition of the ZnO:Al surface window layers for solarcells and other applications through electrohydrodynamic atomization of nanoparticle based ZnO:Al inks has been discussed. The unique advantage which ESD technique carries is that of being a much cheaper and easy solution for the manufacture of photovoltaics at the standard room conditions. The deposited layers present gahnite and zincite structures with good surface morphology and ~250 nm film thickness. The layers give an excellent transparency of more than 90% and a sheet resistivity of 25-36 m_.cm depending upon the sintering temperature ranging from 300 to 500 oC. Thorough characterization of the films has been carried to confirm the structural and compositional integrity of the films.

As far as the future work and future research areas are concerned, it is believed that a lot of room is there. The work in this thesis has been carried out using a single nozzle approach and the deposition area was not more than ~1cm2 which is very small when seen in the backdrop of large area continuous production. Hence it is very important that a multi-nozzle setup containing a large number of nozzles should be deployed. However there are certain challenges in using the multi-nozzle setup, the most important of them being cross-talk between adjacent nozzles [Choi et al 2011, Khan et al. 2012]. Another challenge is that of system design so that a uniform flow distribution occurs. Nanoparticles' entanglement, solvent evaporation and solubility problems also need to be taken care of so that problems like nozzle blockage and non-uniform flow distribution be taken care off. Another area of future research is the problems of a specific electrospray mode control. Electrospray is very sensitive to the liquid physical properties and the electric field in the vicinity of the emitter tip. The issue of continuous control of spray modes has been undertaken by Valaskovic et al. [Valaskovic et al. 2004]. An orthogonal opto-electronic system based on the

spray plume observation in certain characteristic cross sections, which controls the applied voltage has been developed. For further development in MEMS, nanotechnology, and nano-electronics it will be necessary to develop the direct patterning techniques for the deposition of thin layers of pattern size finer than 1 μm.

References

Abou-Rasa et. al. Thin Solid Films. 480-481 433 (2005).

Bjorkmanet. al. Thin Solid Films. 431-432 321 (2003).

Bari et al. Bull. Mater. Sci. 29 529 (2006).

Bindu et. al. Sol. Energ. Mat. Sol. C. 79 67 (2003).

Bakker et. al. Surf. Coat.Tech. 201 9422 (2007).

Chiang and Wager, App. Phys. Lett. 86 013503 (2005).

Chen and Schoonman, J. Ind. Eng. Chem. 10 (7) 1114 (2004).

Choi et. al., Int. J. Adv. Manuf. Technol. 48 165 (2009).

Cloupeau and Prunet-Foch, J. AerosolSci. 24 (6) 1021 (1994).

Cloupeau and Prunet-Foch, J. Electrostatics. 22 135 (1989).

Choi et. al. Jpn. J. Appl. Phys. 49 05EC08 (2010).

Choi et. al. Int. J. Mat. Res. (formerly Z. Metallkd.). 102 310 (2011).

Chung and Troutt, J. Fluid Mech. 186 199 (1988).

Craciunet. al. Appl. Phys. Lett. 65 2963 (1994).

Chen et. al. Mater Chem. 05 765 (1996).

Chen, J. Ind. Eng. Chem. 10 (7) 1114 (2004).

Contreras, Photovoltaics. 7(4) 311 (1999).

Choi et. al. Proc. Inst. Mech. Eng. Part C-J.Eng. Mech. Eng. Sci. 226(3) 842 (2012).

Chen, Mater Chem. 05 765 (1996).

Choi et. al. J. Electrostatics. 69 380 (2011).

Dwivediet. al. J. Ovonic Res. 6 57 (2010).

Ding et. al. Solid State Phenomena. 155 151 (2009).

Eberspacher et al. Thin Solid Films. 387 18 (2001).

Ellmer and Wiendt, Surf. Coat.Technol. 93(1) 21 (1997).

Ganan-Calvo, J. Aerosol Sci. 28 249 (1997).

Guillén and Herrero, J. Appl. Phys. 71(11) 5479 (1992).

Gupta and Isomura, Sol. Energ. Mat. Sol. C. 53 385401 (1998).

Hirvikorpiet. al. Thin Solid Films, 518(10) 2654 (2010).

Hirvikorpiet. al. Thin Solid Films, 518(19) 5463 (2010).

Hartman, Electrohydrodynamic Atomization in the Cone-jet Mode from Physical Modeling to Powder Production.PhD Thesis, TU Delft (2006).

He et. al. J. Phys. Chem. Solids. 64 2075 (2003).

Hermann et. al. Sol. Energ. Mat. Sol. C. 52 355 (1998).

Heoet. al. Appl. Phys. Lett. 85 2274 (2004).

Habibi, J. Sol-Gel Sci. Technol. 54 195 (2010).

Ishikawa and Tsujimura: The Japan Society of Mechanical Engineers 64 (1998).

Jaworek, J. Mater. Sci. 42 266 (2007).

Jaworek and Krupa, J. Aerosol Sci. 30 873 (1999).

Jaworek and Krupa, Trans. Inst. Fluid Flow Mach. 94 155 (1992).

Javed, Turk. J. Phys. 31 287 (2007).

Jaworeket. al. Solid State Phenomena. 140 127 (2008).

Kim et. al. Mat. Manuf. Proc. (DOI:10.1080/10426914.2012.663121– in press).

Kapur et. al. Thin Solid Films. 431–432 53 (2003).

Kaelin et. al. Thin Solid Films. 457 391 (2004).

Kumar et. al. Thin Solid Films 255 2382 (2008).

Kaelin, et. al. Thin Solid Films 516 2188 (2008).

Kumar, Thin Solid Films. 518-24(1) e183 (2010).

Khan et. al. J. Mat. Proc. Technol. 212 700 (2012).

Liakhova et. al. Ferroelectrics, 342(1) 73 (2006).

Liu et. al. Appl. Phys. A. 88 653 (2007).

Liberaet. al. Thin Solid Films. 516-18 6158 (2008).

Mäkeläet. al. Patent #. FI2009/050084 (2009).

Mäkelä, Functional Materials Scientific, 2010, Espoo, Finland

Muhammad et. al. Curr. Appl. Phys. 11 (2011) S68.

Matsubara et. al. Thin Solid Films. 431-432 369 (2003).

Minami et. al. Thin Solid Films 445 268 (2003).

Mitzi, Solution Processing of Inorganic Materials, A. John Wiley & Sons, Inc., New Jersey NJ, 2009.

Musat, Surf. Coat. Technol. 180-181 659 (2004).

Minami, Thin Solid Films. 445-2 268 (2003).

Muhammad, Thin Solid Films. 520 1751 (2012).

Natsumeet. al. Phys. Status Solidi A. 148 485 (1995).

Norris et. al. J. Phys. D. 36 L105 (2003).

Oh et. al. J. Appl. Phys. 99 124505-1 (2005).

Ogata et. al. J. Cryst. Growth. 214 312 (2000).

Poon, Electrohydrodynamic Printing.PhD thesis, Princeton University (2002).

Seeber, Mater. Sci. Semicond. Process. 2 45 (1999).

Sakai, Surf. Coat. Technol. 202(22-23) 5467 (2008).

Samarasinghe et. al. Appl. Phys. A-Mater. Sci. Process. 91 141 (2008).

Song, Appl. Surf. Sci. 254 4171 (2008).

Savadogo, Sol. Energ. Mat. Sol. C. 52 361 (1998).

Sebastian et. al. http://www.sciencedirect.com/science/article/pii/S0927024899000379 - ORFB#ORFBSol. Energ. Mat. Sol. C. 59 125 (1999).

Schmid et. al. http://www.sciencedirect.com/science/article/pii/S0927024899000379 - ORFB#ORFBSol. Energ. Mat. Sol. C. 41-42 281 (1996).

Samarasingheet. al. Appl. Phys. A-Mater. Sci. Process. 91 141 (2008).

Sene et. al.Thin Solid Films. 516(8) 2188 (2008).

Tenhaeff and Gleason, Adv. Func. Mat. 18(7) 979 (2008).

Titus et. al. J. Appl. Phys. 99 043502 (2006).

Valaskovicet. al. J. Am. Soc. Mass Spectrom, 15 1201 (2004).

Volkman, et. al. IEDM Tech. Dig. 7803 (2004).

Wager, Science.300 1245 (2003).

Wang et. al. Appl. Phys. Lett. 86 243503-1 (2005).

Wilhelm, Ph. D. Thesis, Swiss Federal Institute of Technology, Switzerland, (2004).

Wan et. al. Mat.Sci. Eng B 150 203 (2008).

Yoon et. al. Sol. Energ. Mat. Sol. C. 93 783 (2009).

Yee et. al. J. Vac. Sci. Technol. A. 14 1943 (1996).

Yee, J. Vac. Sci. Technol. A. 14 1943 (1996).

Yogamalar and Bose, J. Alloys Compd. 509 8493 (2011).